Dynamic Analysis and Fuzzy Finite-time Optimal Synchronization Control of Unidirectionally Coupled FO Permanent Magnet Synchronous Generator System

Shaohua Luo, Yongduan Song, *Fellow, IEEE*, Frank L. Lewis, *Life Fellow, IEEE*, Roberto Garrappa, Shaobo Li

***Abstract*—This paper focuses on dynamic analysis and the fuzzy finite-time optimal synchronization control problem of unidirectionally coupled fractional-order (FO) permanent magnet synchronous generator (PMSG) system. The synchronization model between FO master and slave PMSGs with capacitive and resistive couplings is built. The dynamic analysis fully reveals its abundant dynamical behaviors including chaotic oscillations and gives stability/instability boundaries with the designed numerical method. In controller design, the hierarchical type-2 fuzzy neural network (HT2FNN) with a transformation is designed to approximate unknown functions, the finite-time command filter matched up with the compensating signal is proposed to achieve precise estimate and fast convergence, and a finite-time preconfigured performance function integrated with a smooth and invertible function is built to realize finite-time convergence and performance constraint. Then a fuzzy finite-time optimal synchronization control scheme fusing with the HT2FNN, filter, performance function and optimal control is developed under the FO backstepping theory. The stability analysis proves that all signals of the closed-loop system are bounded along with the cost function being minimized. Finally, numerical simulation results verify the feasibility and advantages of our scheme.**

***Index Terms*—Unidirectionally coupled FO PMSG system; Dynamical analysis; Fuzzy finite-time optimal synchronization control; Uncertainty; HT2FNN.**

I. Introduction

THE PMSG, which can convert wind energy into mechanical work and output the alternating current by means of mechanical work driving magnetic rotor rotation, is one of key electrical equipment [1-3]. At present, it has been widely applied to high-speed power generation, renewable energy power generation, wind power generation and so on [2-5]. The PMSGs of wind power farms generally work in harsh environments wherein the fluctuations derived from local wind speed, generator temperature, magnetic field, friction and work load are inevitable. These fluctuations may prompt abundant nonlinear dynamics of the PMSG such as chaotic oscillations, multi-stability, snap-through and pull-in. Meanwhile, the fluctuations cause performance degradation of synchronous generator, even damage without taking useful measures. In addition, the requirements on the reliability and security of the PMSG are becoming higher along with the improvement of living standards. Therefore, it is meaningful and challenging to model accurately, reveal stability/instability boundaries of motion and propose a fuzzy finite-time optimal synchronization control scheme between FO master and slave PMSGs within the prescribed performance.

Fractional calculus, in contrast with the traditional integer-order calculus, can provide a more accurate model and a more truly depiction of dynamic characteristics of real systems, whilst tuning the FO system may lead to an optimal dynamic response [6-9]. Westerlund and Ekstam [10] demonstrated FO values for various dielectrics of capacitors by an experiment wherein it had a close FO connection between current flowing and voltage. Luo et al. [11] did an experimental study to testify control performance of FO systems with fractional capacitor membrane models. For modelling and dynamic analysis of FO generators, sporadic works have been reported during past decades. Xu et al. [8] established the FO model of an hydro-turbine- generator unit system and analyzed its nonlinear dynamics with six typical FOs. Borah and Roy [12] analyzed dynamics and presented a single-state predictive control method of the FO PMSG. Ardjal et al. [6] built the FO model and designed a nonlinear synergetic controller for generator and grid converters of a wind energy conversion system. These important results give us some inspirations to current study. However, these models are restricted to a single isolated generator without considering coupling strength between generators, and the corresponding dynamical analysis does not give stability/instability boundaries and regions. Meanwhile, the control issues like finite-time, uncertainty, performance constraint and optimization are not involved.

The synchronization of mutually coupled systems has attracted much attention in nonlinear science, e.g., in the field of the power generation, the synchronization has achieved exact coincidence of frequencies for many generators in parallel mode[13-16]. To better tackle such issue, a large amount of valuable works like robust synchronization [17], adaptive synchronization [18, 19] and optimal synchronization [20, 21] continuously appear. However, these works are confined to integer-order (IO) systems without reference to bi- and uni-directionally coupling strength, and the related systems do not generate complex nonlinear dynamics in the fluctuation which deviates from the discussed syn-

S. Luo is with State Key Laboratory of Public Big Date, Guizhou University, Guiyang 550025, China and also with UTA Research Institute, University of Texas at Arlington, Fort Worth, TX 76118, USA (e-mail: shluo@gzu.edu.cn).

Y. Song is with State Key Laboratory of Power Transmission Equipment & System Security and New Technology and School of Automation, Chongqing University, Chongqing 400044, China and also with Start Institute of Intelligent Systems (SIIS), Chongqing 400044, China (e-mail: ydsong@cqu.edu.cn).

F. Lewis is with UTA Research Institute, University of Texas at Arlington, Fort Worth, TX 76118, USA (e-mail: lewis@uta.edu).

R. Garrappa is with Department of Mathematics, University of Bari, Bari 70126, Italy (e-mail: roberto.garrappa@uniba.it).

S. Li is with State Key Laboratory of Public Big Date, Guizhou University, Guiyang 550025, China (e-mail: lishaobo@gzu.edu.cn).

This is the preprint of the paper
S.Luo, F.L. Lewis, Y.Song, R.Garrappa, S.Li
Dynamic Analysis and Fuzzy Fixed-Time Optimal Synchronization Control of Unidirectionally Coupled FO Permanent Magnet Synchronous Generator System, IEEE Transactions on Fuzzy Systems, 2023, 31(5), 1743-1755 - doi: 10.1109/TFUZZ.2022.3213977

chronization. Sadeghi et al. [22] solved a smooth synchronization problem of brushless doubly-fed induction generator by using a machine model. Zhu et al. [15] studied the synchronization of chaotic-oscillation PMSG networks by using an adaptive impulsive control scheme. The above literature did not reveal chaotic and regular regions of generators in the field of integer calculus. Meanwhile the parameters perturbations and uncertainties of system modelling inevitably result in failure of these schemes in the absence of preconfigured performance.

As an effective tool, the backstepping control is widely applied to IO uncertain nonlinear systems by fusing fuzzy logic systems (FLS) or neural networks (NN) [23-25]. Some researchers have extended it to the FO filed [26, 27]. Aimed to the 'explosion of complexity' of backstepping, the first-order low-pass filter, tracking differentiator and observer are adopted to tackle this issue whether it belongs to the IO or FO field. It is undeniable that these works provide reference for our study. But the coupled PMSG is completely different from a class of nonlinear mathematical models wherein it does not produce undesired dynamical behaviors like chaotic oscillations and multi-stability, and the issue associated with the fuzzy finite-time optimal synchronization control is not mentioned above. The optimal control has become an important research topic by virtue of consuming fewer resources [28-30]. Some researchers incorporate it into the backstepping to control nonlinear systems [30, 31], in which their respective advantages are brought into full play. The finite-time control of nonlinear systems is regarded as an interesting research topic because of fast response and high convergence accuracy [32, 33]. The unidirectionally coupled FO PMSG system is a highly complex system with coupling strength from the surrounding generators in wind power plant. How to fuse these useful methods like optimal control, backstepping and finite-time control and put forward a fuzzy finite-time optimal synchronization control scheme of unidirectionally coupled PMSG system to reach the prescribed performances is still an outstanding issue in FO field.

Motivated by the above observations, in this work we build the synchronization model of unidirectionally coupled FO PMSGs, analyze its dynamical characteristics and then propose a fuzzy finite-time optimal synchronization control scheme. The presented synchronization control scheme is developed by highly integrating the HT2FNN, finite-time command filter, finite-time preconfigured performance function and optimal control on the basis of the backstepping.

The main contributions of this paper are summarized as follows.

Firstly, comparing with [15, 34], we establish the synchronization model of unidirectionally coupled FO PMSGs to reach order and harmony of their behaviors rather than the IO model of isolated PMSG. It can give an exact description of dynamic characteristics of the system and increase design freedom. Meanwhile, the dynamic analysis fully reveals stability/instability boundaries versus time and shows the tendency toward chaotic/regular motions versus parameters combination with the constructed numerical method.

Secondly, our scheme solves the 'explosion of complexity' of backstepping existed in [24, 25], even in higher order systems, tackles infinite time convergence in a form of exponential form and non-adjustable convergence speed between initial phase and homeostasis phase in [35, 36], and provides greater flexibility and better functional properties along with a comparison with ordinary FLS and NN in [23-25].

Thirdly, unlike [28-30, 37], this work achieves the fuzzy finite-time optimal synchronization control of unidirectionally coupled FO PMSG system along with solving finite-time convergence, unknown system functions, conformity of preset constraint conditions and minimum of cost function in the framework of FO backstepping.

II. System modeling and preliminaries

A. Preliminaries

Definition 1 [38, 39]: For a sufficiently differentiable function $F(t)$, the Caputo fractional derivative can be written

$$ {}^{C}\mathscr{D}_{0,t}^{\alpha}F(t)=\frac{1}{\Gamma(n-\alpha)}\int_0^t\frac{F^{(n)}(\tau)}{(t-\tau)^{1-n+\alpha}}\mathrm{d}\tau, \tag{1}$$

where $\Gamma(n-\alpha)=\int_0^\infty e^{-t}t^{n-\alpha-1}\mathrm{d}t$ is called the Euler-Gamma function with $n-1<\alpha<n$ and $n\in\mathbb{N}_+$.

Using a Laplace transform for (1), it is obtained

$$\mathbf{L}\left\{ {}^{C}\mathscr{D}_{0,t}^{\alpha}F(t)\right\}=s^{\alpha}\mathbf{L}\left\{F(t)\right\}-\sum_{k=0}^{n-1}\frac{F^{(k)}(0)}{s^{k+1-\alpha}}. \tag{2}$$

For any continuous functions $F_1(t)$ and $F_2(t)$ in the interval $[0,t_\varsigma]$ under $0<\alpha<1$, there exists

$$F_1(t)\cdot{}^{C}\mathscr{D}_{0,t}^{\alpha}F_2(t)+F_2(t)\cdot{}^{C}\mathscr{D}_{0,t}^{\alpha}F_1(t)={}^{C}\mathscr{D}_{0,t}^{\alpha}\left(F_1(t)\cdot F_2(t)\right)+$$
$$\frac{\alpha}{\Gamma(1-\alpha)}\int_0^t\frac{1}{(t-\varsigma)^{1-\alpha}}\left(\int_0^\varsigma\frac{F_1'(\varsigma_1)d\varsigma_1}{(t-\varsigma_1)^{\alpha}}\cdot\int_0^\varsigma\frac{F_2'(\varsigma_2)d\varsigma_2}{(t-\varsigma_2)^{\alpha}}\right)\mathrm{d}\varsigma. \tag{3}$$

As $F_1(t)=F_2(t)$, the following inequality is easily deduced

$$ {}^{C}\mathscr{D}_{0,t}^{\alpha}\left(F^2(t)\right)\le 2F(t)\cdot{}^{C}\mathscr{D}_{0,t}^{\alpha}F(t). \tag{4}$$

Lemma 1[40]: For any $x_s, y_s\in\mathbb{R}$, if the constants $c_s>0$, $d_s>0$ and $\vartheta(x_s,y_s)$ is any positive real function, the inequality holds

$$|x_s|^{c_s}|y_s|^{d_s}\le\frac{c_s\vartheta(x_s,y_s)|x_s|^{c_s+d_s}}{c_s+d_s}+\frac{d_s\vartheta(x_s,y_s)^{-\frac{c_s}{d_s}}|y_s|^{c_s+d_s}}{c_s+d_s}. \tag{5}$$

Definition 2 [28, 41] : A performance cost function which needs to be minimized is given as

$$\bar{J}=\int_0^\infty\left(\bar{Q}\left(\bar{S}(t)\right)+U^{\mathrm{T}}\bar{\mathrm{R}}U\right)\mathrm{d}t, \tag{6}$$

where $\bar{S}$, U and $\bar{\mathrm{R}}$ represent the penalty function, optimal control input and N-order matrix, respectively, $\bar{Q}(\bar{S})>0$.

B. Synchronization modeling of the PMSGs

As is shown in Fig.1, the wind energy conversion system usually consists of a wind turbine, a PMSG and three converters which are a diode bridge rectifier, a dc/dc boost converter and an inverter in the order. The electric power originated from the PMSG is transferred to the grid by the mentioned converters.

Based on the local aerodynamic characteristics, the wind turbine can generate the power which is expressed as

$$P_w=\frac{1}{2}\rho\pi C_p\left(\omega_r R/v_w,\beta\right)R^2v_w^3, \tag{7}$$

where ρ, R, ω_r, β, ω_r and v_w denote the air density, turbine radius, rotor speed, blade pitch angle, rotor speed and wind speed, respectively, $C_p\left(\omega_r R/v_w,\beta\right)$ represents the turbine power coefficient.

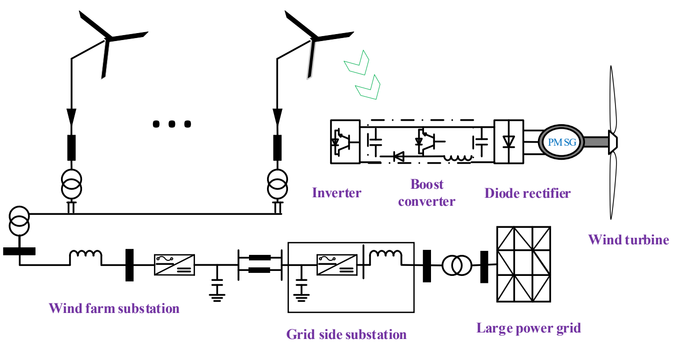

Fig.1. The schematic diagram of the wind energy conversion system.

According to law of rotation, the mechanical FO model of the PMSG is given

$$J\frac{d^{\alpha}\omega_r}{d\tilde{t}^{\alpha}}=T_g-b\omega_r-T_t, \tag{8}$$

where α , J , T_t , T_g , $\tilde{t}$ and b denote the FO coefficient, system inertia, turbine torque, generator torque, time and viscous friction coefficient, respectively.

The electromagnetic generator torque can be defined

$$T_g=\frac{3}{2}p\left(\left(L_q-L_d\right)i_d i_q+i_q\phi\right), \tag{9}$$

where L_d and L_q denote d- and q-axis inductance, i_d and i_q represent d- and q-axis stator current, p and ϕ are the number of pole pairs and magnetic flux of permanent magnet in the three-phase PMSG.

The electrical FO model of the PMSG in the synchronous rotating d-q reference frame is expressed as

$$\begin{cases}\dfrac{d^{\alpha}i_d}{d\tilde{t}^{\alpha}}=\left(-R_s i_d+\omega_r L_q i_q+V_d\right)/L_d,\\ \dfrac{d^{\alpha}i_q}{d\tilde{t}^{\alpha}}=\left(-R_s i_q-\left(L_d i_d+\phi\right)\omega_r+V_q\right)/L_q,\end{cases} \tag{10}$$

where R_s , V_d and V_q denote the stator resistance, d- and q-axis stator voltage.

In the Laplace domain, the following transfer function which has a slope of -20m dB/decade in the Bode diagram can represent the fractional integrator in a form of linear approximation by using pole-zero pairs as

$$\mathbf{F}(s)=\frac{1}{s^{\alpha}}\approx\prod\nolimits_{i=0}^{N_f-1}\left(1+s/Q_i\right)\Big/\prod\nolimits_{i=0}^{N_f-1}\left(1+s/P_i\right), \tag{11}$$

where $N_f=\text{integer}\left(\dfrac{\log\left(\omega_{\max}/p_f\right)}{\log\left(10^{d_f/10(1-\alpha)}\cdot 10^{d_f/10\alpha}\right)}\right)+1$, P_f , $\omega_{\max}$ and d_f denote the corner frequency, frequency bandwidth and discrepancy between actual and approximate lines, respectively, Q_i and P_i represent the zero and pole of the singularity function.

Note $L=L_d=L_q$ because of the stator winding symmetry. With (8) and (10), the FO model of the PMSG is defined as

$$\begin{cases}{}^{C}\mathscr{D}_{0,t}^{\alpha}\omega_r=\left(3p\phi i_q/2-b\omega_r-T_t\right)/J,\\ {}^{C}\mathscr{D}_{0,t}^{\alpha}i_q=\left(-R_s i_q-\left(Li_d+\phi\right)\omega_r+V_q\right)/L,\\ {}^{C}\mathscr{D}_{0,t}^{\alpha}i_d=\left(-R_s i_d+\omega_r Li_q+V_d\right)/L,\end{cases} \tag{12}$$

where ${}^{C}\mathscr{D}_{0,t}^{\alpha}$ is the Caputo derivative of FO $\alpha>0$ with starting point at the origin.

By introducing new variables $x_1=L\omega_r/R_s$, $x_2=pL\phi i_q/bR_s$ and $x_3=pL\phi i_d/bR_s$, the normalized FO model of the master PMSG is written

$$\begin{cases}{}^{C}\mathscr{D}_{0,t}^{\alpha}x_1=\sigma x_2-\rho x_1+T_L,\\ {}^{C}\mathscr{D}_{0,t}^{\alpha}x_2=-x_2-x_1x_3+\mu x_1+u_q,\\ {}^{C}\mathscr{D}_{0,t}^{\alpha}x_3=-x_3+x_1x_2+u_d,\end{cases} \tag{13}$$

where $t=\tilde{t}R_s/L$, $u_q=pL\phi V_q/bR_s^2$, $u_d=pL\phi V_d/bR_s^2$, $T_L=-L^2T_t/JR_s^2$, $\mu=-p\phi^2/bR_s$, $\sigma=3Lb/2JR_s$, $\rho=bL/JR_s$ with x_1 , x_2 , x_3 , t , u_q , u_d , T_L being the normalized angular speed, q-axis current, d-axis current, time, q-axis voltage, d-axis voltage and load torque, respectively, and σ , ρ , μ being the system parameters.

Using the Heaviside function $H\left(t-T_g\right)$, the FO model of the slave PMSG is given

$$\begin{cases}{}^{C}\mathscr{D}_{0,t}^{\alpha}y_1=\sigma y_2-\rho y_1+T_L,\\ {}^{C}\mathscr{D}_{0,t}^{\alpha}y_2=-y_2-y_1y_3+\mu y_1-\left(\boldsymbol{\kappa}_1\left(y_1-x_1\right)+\boldsymbol{\kappa}_2\left(y_2-x_2\right)\right)\\ \cdot H\left(t-t_g\right)+u_q+u_2,\\ {}^{C}\mathscr{D}_{0,t}^{\alpha}y_3=-y_3+y_1y_2+u_d+u_3,\end{cases} \tag{14}$$

where t_g , $\boldsymbol{\kappa}_1$ and $\boldsymbol{\kappa}_2$ denote the initial synchronization time, capacitive coupling and resistive coupling, respectively, u_2 and u_3 denote control inputs.

Define the synchronization errors that $e_1=y_1-x_1$, $e_2=y_2-x_2$ and $e_3=y_3-x_3$. Subtracting (13) from (14) yields

$$\begin{cases}{}^{C}\mathscr{D}_{0,t}^{\alpha}e_1=\sigma e_2-\rho e_1,\\ {}^{C}\mathscr{D}_{0,t}^{\alpha}e_2=-e_2-y_1y_3+x_1x_3+\mu e_1-\left(\boldsymbol{\kappa}_1e_1+\boldsymbol{\kappa}_2e_2\right)H\left(t-t_g\right)+u_2,\\ {}^{C}\mathscr{D}_{0,t}^{\alpha}e_3=-e_3+y_1y_2-x_1x_2+u_3.\end{cases} \tag{15}$$

III. Dynamical analysis and problem formulation

To study dynamical characteristics of the FO master/slave PMSG, a dynamical analysis is performed in this section. Since solutions of nonlinear fractional differential equations (FDEs) are usually not available in an explicit formulation, a numerical approach, based on product-integration rules [39, 42], is studied in this work to solve the nonlinear FO system.

For a generic FDE ${}^{C}\mathscr{D}_{0,t}^{\alpha}y_f\left(t\right)=g\left(t,y_f\left(t\right)\right)$ with $g\left(\cdot,\cdot\right)$ a given function, the difference quotient definition of α th derivative for $y_f\left(t\right)$ can be written in terms of an infinite series

$${}^{C}\mathscr{D}_{0,t}^{\alpha}y_f\left(t\right)=\lim_{h\to 0}\frac{1}{h^{\alpha}}\sum_{j=0}^{\lfloor t/h\rfloor}\omega_j^{(\alpha)}\left(y_f\left(t-jh\right)-y_f\left(0\right)\right),\ \omega_j^{(\alpha)}=\left(-1\right)^j\binom{\alpha}{j}, \tag{16}$$

where $h>0$ and $\omega_j^{(\alpha)}$ denote the step-size and coefficient satisfied the following condition by the aid of the Euler-Gamma function

$$\binom{\alpha}{j}=\begin{cases}\Gamma\left(\alpha+1\right)/\Gamma\left(\alpha+1-j\right)j! & j=0,\cdots,\alpha,\\ 0 & j>\alpha.\end{cases} \tag{17}$$

Define an equispaced grid $t_n = nh$, $n = 0, 1, \cdots, \mathbf{N}$ in the interval $[0, T]$, where $\mathbf{N} = T/h$. Then the integral representation of the solution at $t = t_n$ can hence be given

$$y_f(t_n) = y_{f_0} + \frac{1}{\Gamma(\alpha)} \sum_{j=0}^{n-1} \int_{t_j}^{t_{j+1}} (t_n - \tau)^{\alpha-1} g(\tau, y_f(\tau)) d\tau . \qquad (18)$$

Let a constant $g(t_j, y_{f_j})$ approximate the vector field $g(\tau, y_f(\tau))$ in each subinterval $[t_j, t_{j+1}]$. The evaluation of the resulting integrals in (18) leads to the numerical approximation

$$y_f(t_n) = y_{f_0} + h^{\alpha} \sum_{j=0}^{n-1} \frac{\left((n-j)^{\alpha} - (n-j-1)^{\alpha}\right)}{\Gamma(\alpha+1)} g(t_j, y_{f_j}) . \qquad (19)$$

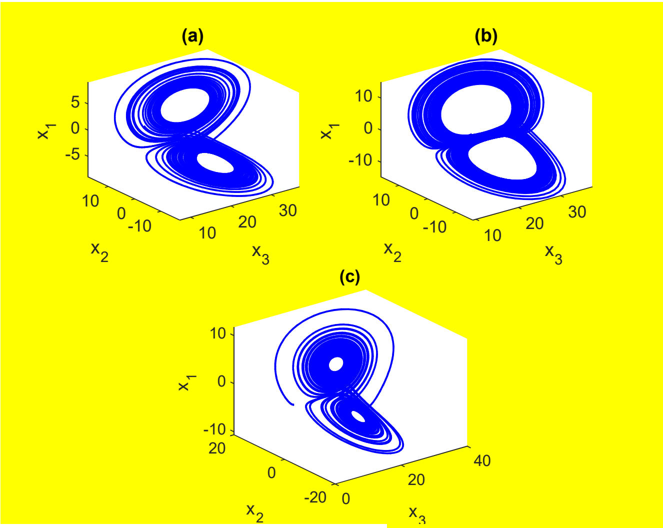

Fig.2. Chaotic phase portraits under three cases ((a) [x1, x2, x3]=[0.1,0.9,20], σ =3, ρ =4, μ =25; (b) [x1, x2, x3]=[1.5,0.5,20], σ =17, ρ =16, μ =25; (c) [x1, x2, x3]= [0.1,0.1, 3], σ =5.5, ρ =5.5, μ =20).

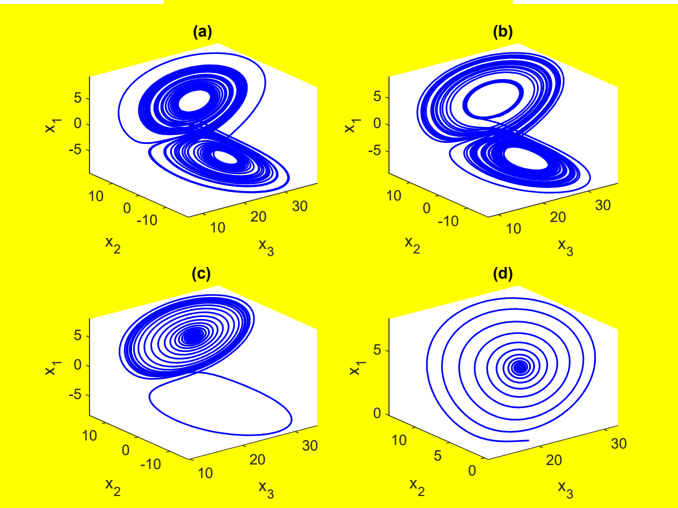

Fig.3. Chaotic phase portraits with Case 1 under varying FOs ((a) α =0.998; (b) α = 0.992; (c) α =0.97; (d) α =0.96).

The system parameters of the FO model for the master/slave PMSG are set to three cases:

Case 1: $\alpha = 0.99$, $\sigma = 3$, $\rho = 4$, $\mu = 25$ and $T_L = 0$ with initial conditions $x_1(0) = 0.1$, $x_2(0) = 0.9$, $x_3(0) = 20$;

Case 2: $\alpha = 0.99$, $\sigma = 17$, $\rho = 16$, $\mu = 25$ and $T_L = 0$ with initial conditions $x_1(0) = 1.5$, $x_2(0) = 0.5$, $x_3(0) = 20$;

Case 3: $\alpha = 0.99$, $\sigma = 5.5$, $\rho = 5.5$, $\mu = 20$ and $T_L = 0$ with initial conditions $x_1(0) = 0.1$, $x_2(0) = 0.1$, $x_3(0) = 3$.

By invoking (11), the approximating transfer functions of different FOs are given such as

$$\frac{1}{s^{0.998}} = \frac{9.95405(1+9.65984\times10^{-10}s)(1+9.8853\times10^{-5}s)}{(1+9.43952\times10^{-10}s)(1+9.65984\times10^{-5}s)(1+9.8853s)}, \qquad (20)$$

$$\frac{1}{s^{0.992}} = \frac{9.81748(1+9.32735\times10^{-5}s)(1+0.0308972s)}{(1+8.90424\times10^{-5}s)(1+0.0294957s)(1+9.77056s)}, \qquad (21)$$

$$\frac{1}{s^{0.98}} = \frac{9.54993(1+7.90604\times10^{-6}s)(1+0.000868511s)(1+0.0954095s)}{(1+7.19686\times10^{-6}s)(1+0.000790604s)(1+0.0868511s)(1+9.54s)}, \qquad (22)$$

wherein the errors value are ≤ 0.1, ≤ 0.2 and ≤ 0.4 dB, respectively.

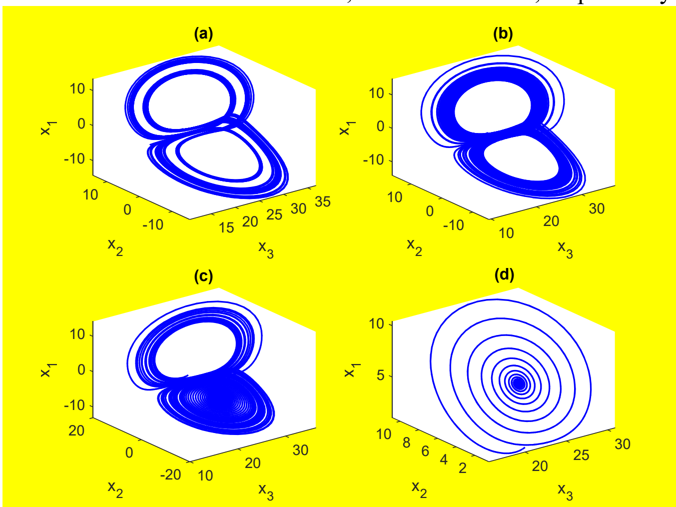

Fig.4. Chaotic phase portraits with Case 2 under varying FOs((a) α =0.998; (b) α = 0.992; (c) α =0.98; (d) α =0.96).

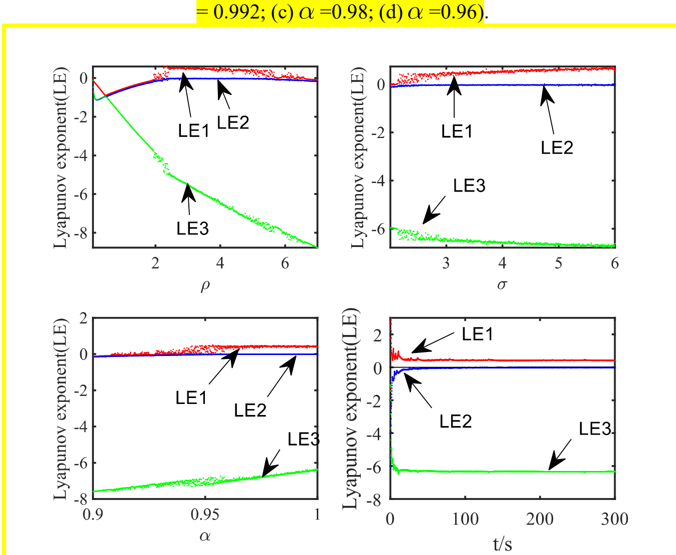

Fig.5. Lyapunov exponents versus system parameters (σ, ρ), FO and time under Case 1.

Obviously, it can be seen from three subgraphs of Fig.2 that the PMSG generates chaotic oscillation with two attractors under the mentioned cases. To show superiority of the FO model and reveal dynamic characteristics of the PMSG associated with FO value, the related chaotic phase portraits with varying FOs under Cases 1-2 are presented in Figs.3-4. Adjustment of FO α to 0.96 makes the periodic motion of the PMSG switch to chaotic orbit with an attractor for both Cases 1-2. As $\alpha = 0.97$ in Case 1, two motion states of the system occur: a period-T behavior and a chaotic attractor. And $\alpha = 0.98$ in Case 2, the motion behaviors of the PMSG turn into chaotic oscillation with two attractors. Then the system motion states stay in chaotic oscillation with two attractors once α is increased to 0.992 or 0. 998, whether it's the Case 1 or Case 2.

Figs.5-6 exhibit the Lyapunov exponents versus system parameters (σ, ρ), FO and time under the mentioned two cases. In the first subgraph of Fig.5, the PMSG falls into the trap of chaotic oscillation as $\rho \in (2, 6.5)$. In its second subgraph, this generator is trapped in chaotic behavior when σ is set to the interval [2.1, 6]. The third subgraph of Fig.5 reveals the rule that the value of the FO triggers chaotic oscillation in (0.912,1). The last subgraphs of Figs.5-6 show that the PMSG enters in chaos during the whole process. In the first subgraph of Fig.6, the PMSG is in a state of chaos as $\rho \in (2, 16)$. Note there exists a switch point between periodic state and chaotic vibration. In the corresponding second subgraph, the PMSG turns into chaotic vibration when σ belongs the interval [12.4, 20]. The third subgraph of Fig.6 presents that the value of the FO can give rise to chaos from $\alpha > 0.928$.

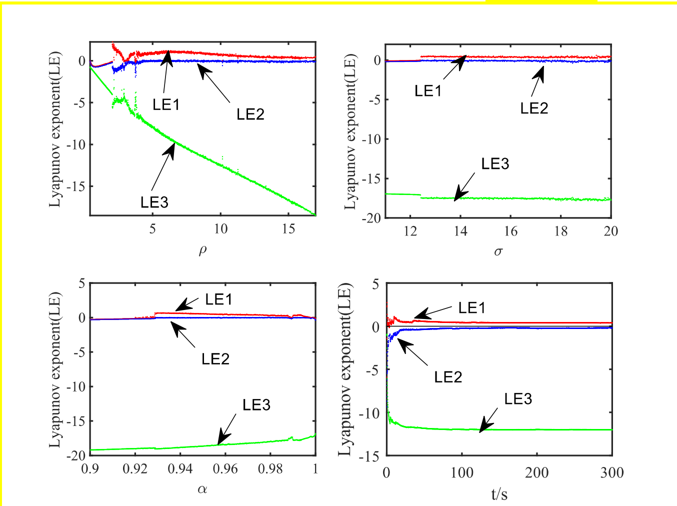

Fig.6. Lyapunov exponents versus system parameters (σ, ρ), FO and time under Case 2.

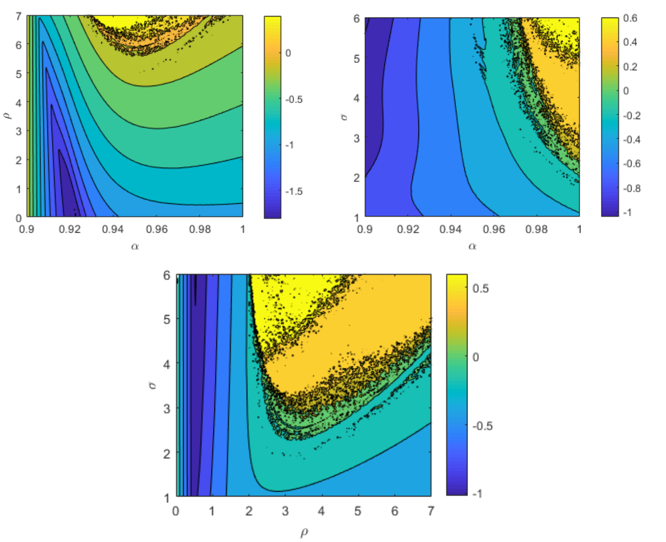

Fig.7. The contour plots of the maximum Lyapunov exponents associated with chaotic oscillations in $\alpha - \rho$, $\alpha - \sigma$ and $\sigma - \rho$ parameters planes under Case 1.

Figs.7-8 show the contour plots of the maximum Lyapunov exponents concerned with stability/instability boundaries in the $\alpha - \rho$, $\alpha - \sigma$ and $\sigma - \rho$ parameters planes under Cases 1-2. The colorbar of each subgraph is displayed to indicate the interval of generating chaos between two parameters such as $\alpha - \rho$, $\alpha - \sigma$ and $\sigma - \rho$. It can be obviously seen that the field of lemon yellow has the maximum Lyapunov exponent. This is to say, the combination of three parameters falls into the field of lemon yellow, then the PMSG can produce chaotic oscillation. This oscillation has many application scenarios. But for the PMSG, the such oscillation can lead to performance reduction of the running system, even burn the generator with components around it. Therefore, it is necessary to propose an effective scheme to suppress chaotic oscillation.

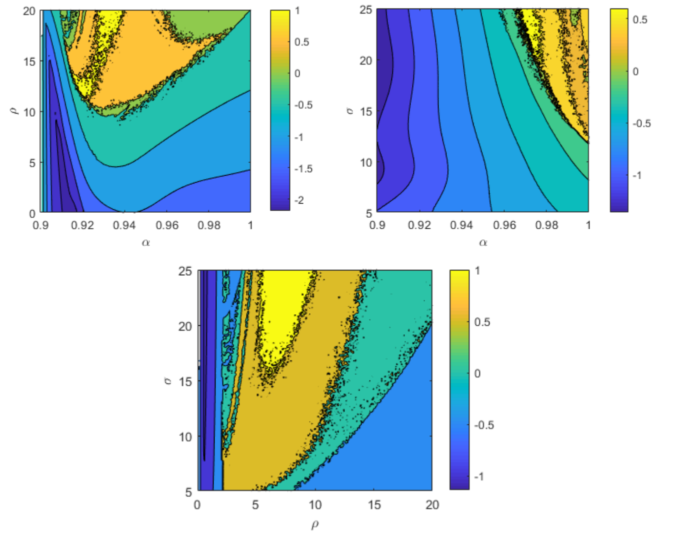

Fig.8. The contour plots of the maximum Lyapunov exponents associated with chaotic oscillations in $\alpha - \rho$, $\alpha - \sigma$ and $\sigma - \rho$ parameters planes under Case 2.

Remark 1: According to the abovementioned contents, the constructed FO model simply and accurately describes the process of historical memory and global spatial correlation for the PMSG compared with the IO one. If $\alpha = 1$, $\boldsymbol{\kappa}_1 = \boldsymbol{\kappa}_2 = 0$ and $\sigma = \rho$, this model can degrade to the cases in [15, 34].

Meanwhile, the type-1 FNN faces a problem of poor approximation precision for high-dimensional hyper-chaotic systems, and how to further improve the stabilization time and dynamic performance of unidirectionally coupled FO PMSGs is tricky along with minimizing the cost function.

For these reasons, the control object of this paper is formulated: for the synchronization model of unidirectionally coupled FO PMSGs, propose a fuzzy finite-time optimal synchronization control scheme such that all signals in the closed-loop system are bounded and the synchronization error converges to zero in the finite-time and pregiven constraint condition.

IV. Fuzzy finite-time optimal controller design

A. Hierarchical type-2 fuzzy neural network

The HT2FNN, which is the derivant of type-1 FNN, possesses strong ability in the field of learning, function approximation and fault tolerance [41, 43, 44]. It is made up of five layers such as input layer, membership layer, rule layer, type-reduction layer and output layer. In the second layer, the upper and lower membership grades (MGs) can be written

$$\overline{\mu}_{\tilde{A}_i^j}(x_i) = \exp\left(-\left(\left(x_i - m_{\tilde{A}_i^j}\right)/\overline{\sigma}_{\tilde{A}_i^j}\right)^2/2\right),$$

$$\underline{\mu}_{\tilde{A}_i^j}\left(x_i\right)=\exp\left(-\left(\left(x_i-m_{\tilde{A}_i^j}\right)/\underline{\sigma}_{\tilde{A}_i^j}\right)^2/2\right), i=1,\cdots,N, \quad (23)$$

where $m_{\tilde{A}_i^j}$, $\bar{\sigma}_{\tilde{A}_i^j}$ and $\underline{\sigma}_{\tilde{A}_i^j}$ denote the center, upper width and lower width of the j-th MGs for i-th input, respectively.

In the rule layer, the upper/lower rule firing is computed as

$$\bar{T}_{ac}^j=\bar{\mu}_{\tilde{A}_1^a}\left(x_1\right)\bar{\mu}_{\tilde{A}_2^\varsigma}\left(x_2\right),\ \underline{T}_{ac}^j=\underline{\mu}_{\tilde{A}_1^a}\left(x_1\right)\underline{\mu}_{\tilde{A}_2^\varsigma}\left(x_2\right). \quad (24)$$

In the fourth layer, Y_R and Y_L can be expressed in terms of the center of sets type reduction

$$Y_R=\frac{\sum_{j=1}^{M}R^j\underline{T}^jw_R^j+\sum_{j=r+1}^{M}\left(1-R^j\right)\bar{T}^jw_R^j}{\sum_{j=1}^{M}R^j\underline{T}^j+\sum_{j=r+1}^{M}\left(1-R^j\right)\bar{T}^j},$$

$$Y_L=\frac{\sum_{j=1}^{M}L^j\bar{T}^jw_L^j+\sum_{j=l+1}^{M}\left(1-L^j\right)\underline{T}^jw_L^j}{\sum_{j=1}^{M}L^j\bar{T}^j+\sum_{j=l+1}^{M}\left(1-L^j\right)\underline{T}^j}, \quad (25)$$

where w_R^j and w_L^j are called as the weight, $\underline{T}^j$ and $\bar{T}^j$ denote the lower and upper firing degrees of j-th rule, M is the number of fuzzy rules, $R\equiv\left[\underset{1}{\underset{\downarrow}{1}}\cdots\underset{r}{\underset{\downarrow}{1}}\ \underset{r+1}{\underset{\downarrow}{0}}\cdots\underset{M}{\underset{\downarrow}{0}}\right]\in\mathbb{R}^M$ and $L\equiv\left[\underset{1}{\underset{\downarrow}{1}}\cdots\underset{l}{\underset{\downarrow}{1}}\ \underset{l+1}{\underset{\downarrow}{0}}\cdots\underset{M}{\underset{\downarrow}{0}}\right]\in\mathbb{R}^M$.

In output layer, the defuzzified output in vector form is deduced

$$Y=w^{\mathrm{T}}\xi=w_R^{\mathrm{T}}\xi_R+w_L^{\mathrm{T}}\xi_L, \quad (26)$$

with $w\equiv\left[w_R,w_L\right]$, $w_R\equiv\frac{1}{2}\left[w_R^1\cdots w_R^M\right]^{\mathrm{T}}$, $w_L\equiv\frac{1}{2}\left[w_L^1\cdots w_L^M\right]^{\mathrm{T}}$, ξ_R

$$\equiv\left[\frac{R^1\underline{T}^1+\left(1-R^1\right)\bar{T}^1}{\sum_{j=1}^{M}R^j\underline{T}^j+\sum_{j=r+1}^{M}\left(1-R^j\right)\bar{T}^j}\cdots\frac{R^M\underline{T}^M+\left(1-R^M\right)\bar{T}^M}{\sum_{j=1}^{M}R^j\underline{T}^j+\sum_{j=r+1}^{M}\left(1-R^j\right)\bar{T}^j}\right]^{\mathrm{T}},$$

$$\xi_L\equiv\left[\frac{L^1\underline{T}^1+\left(1-L^1\right)\bar{T}^1}{\sum_{j=1}^{M}L^j\underline{T}^j+\sum_{j=r+1}^{M}\left(1-L^j\right)\bar{T}^j}\cdots\frac{L^M\underline{T}^M+\left(1-L^M\right)\bar{T}^M}{\sum_{j=1}^{M}L^j\underline{T}^j+\sum_{j=r+1}^{M}\left(1-L^j\right)\bar{T}^j}\right]^{\mathrm{T}},$$

$\xi\equiv\left[\xi_R,\xi_L\right]$.

By invoking (26), the HT2FNN can realize the approximation for any unknown but bounded function h with high precision over a compact set as

$$\sup_{X\in D_X}\left|h\left(X\right)-w^{\mathrm{T}}\xi\left(X\right)\right|\le\varepsilon\left(X\right), \quad (27)$$

where $X\equiv\left[x_1\cdots x_i\right]^{\mathrm{T}}\in\mathbb{R}^i, i=1\cdots N$ with N denoting input number, $\varepsilon\left(X\right)>0$ is the approximation error, Ω_w and D_X are the compact sets of suitable bounds of w and X, respectively. Introduce an optimal parameter w^* which meets the condition as $\arg\min_{w\in\Omega_w}\left[\sup_{X\in D_X}\left|h\left(X\right)-\hat{h}\left(X,w\right)\right|\right]$ with $\hat{h}$ being the approximation of h. Let $\tilde{w}=w-w^*$ in which w^* denotes an artificial quantity used for analysis.

To refrain the exponential growth of the rule number, two criteria (decreasing rate of tracking error and ε-completeness of fuzzy rules) are performed to echo with structure adjustment of the HT2FNN. The decreasing rate of tracking error is equivalent to the derivative of the tracking error square between outputs of drive and response systems. The ε-completeness of fuzzy rules is defined as 'there is at least a fuzzy rule to guarantee that the firing strength is not less than ε in the operation range'. If the MGs are equal or greater than 0.5 in hierarchical form, save them. Otherwise, delete these unimportant rules in self-structuring algorithm.

To improve solution speed and simplify structure, a transformation associated with the HT2FNN is given

$$w^{\mathrm{T}}\xi\left(X\right)\le\zeta\xi^{\mathrm{T}}\left(X\right)\xi\left(X\right)/2b^2+b^2/2, \quad (28)$$

where $\zeta=\|w\|^2$ and $b>0$. There exists $\tilde{\zeta}=\zeta-\hat{\zeta}$ in which $\hat{\zeta}$ is the estimation of ζ.

Remark 2: Compared with the Grunwald–Letnikov and Riemann–Liouville derivatives, the initial conditions of FO differential equations with the Caputo derivative have the same form as those for IO differential equations. Meanwhile, the Caputo derivative possesses a value of zero when it is applied to a constant. Therefore, it can directly deduce that ${}^{C}\mathscr{D}_{0,t}^{\alpha}\tilde{\zeta}=-{}^{C}\mathscr{D}_{0,t}^{\alpha}\hat{\zeta}$.

Remark 3: Comparing with type-1 FNN, the HT2FNN lift restrictions for precise and crisp membership functions. The membership functions of type-2 fuzzy sets are three dimensional and include a footprint of uncertainty. The HT2FNN provides additional degrees of freedom which makes it possible to directly model and handle uncertainties.

B. Controller Design

To avoid performance degradation of system and restrain convergent characteristic of error variables, a finite-time preconfigured performance function (FPPF) which is positive and strictly monotonic decreasing can be designed

$$\beta\left(t\right)=\begin{cases}a_3t^3+a_2t^2+a_1t+a_0, & t\in\left[0,T_0\right)\\ \beta_{T_0}, & t\ge T_0\end{cases} \quad (29)$$

where $a_i, i=0,\cdots,3$ denote design parameters, T_0 and β_{T_0} mean the convergence time and convergence boundary. Meanwhile, this performance function satisfies the following constraint conditions

$$\begin{cases}\beta\left(0\right)=\beta_0,\ {}^{C}\mathscr{D}^{\alpha}\beta\left(0\right)=0,\\ \beta\left(t\middle|t\ge T_0\right)=\beta_{T_0},\ {}^{C}\mathscr{D}^{\alpha}\beta\left(t\middle|t\ge T_0\right)=0,\end{cases} \quad (30)$$

where β_0 denotes initial condition of the finite-time preconfigured performance function.

Remark 4: The constraint conditions suppress a large overshoot of control output in the initial stage when the constrained signals match up with the convergence rate of the preconfigured performance function. For the pre-given parameters such as β_0, T_0 and β_{T_0}, it is easy to obtain a satisfactory finite-time preconfigured performance function by appropriately choosing four design parameters.

To realize the faster response, the FO finite-time command filter originated from a first-order Levant differentiator [45] is given

$$\begin{cases}{}^{C}\mathscr{D}_{0,t}^{\alpha}\mathrm{Z}_{i,1}=\bar{\mathbf{Z}}_{i,1},\ \bar{\mathbf{Z}}_{i,1}=-\boldsymbol{c}_{i,1}\left|\mathrm{Z}_{i,1}-\alpha_r\right|^{\frac{1}{2}}\operatorname{sign}\left(\mathrm{Z}_{i,1}-\alpha_r\right)+\mathrm{Z}_{i,2}\\ {}^{C}\mathscr{D}_{0,t}^{\alpha}\mathrm{Z}_{i,2}=-\boldsymbol{c}_{i,2}\operatorname{sign}\left(\mathrm{Z}_{i,2}-\bar{\mathbf{Z}}_{i,1}\right), i=1,\cdots,N\end{cases} \quad (31)$$

where $Z_{i,1} \in \mathbb{R}$ and $Z_{i,2} \in \mathbb{R}$ are command filter states, $\alpha_r \in \mathbb{R}$ is input signal of this filter, and $\boldsymbol{c}_{i,1}$ and $\boldsymbol{c}_{i,2}$ denote positive design constants. There exists positive constants $\Gamma_{i,1}$ and $\Gamma_{i,2}$ satisfying $\left|Z_{i,1}-\alpha_r\right| \le \Gamma_{i,1}$ and $\left|\bar{\mathbf{Z}}_{i,1} - {}^{C}\mathscr{D}_{0,t}^{\alpha}\alpha_r\right| \le \Gamma_{i,2}$.

It should be clear here that by appropriate selections of $\boldsymbol{c}_{i,1}$ and $\boldsymbol{c}_{i,2}$, $Z_{i,1}=\alpha_r$ and $\bar{\mathbf{Z}}_{i,1} = {}^{C}\mathscr{D}_{0,t}^{\alpha}\alpha_r$.

Introduce error variables

$$z_2 = e_2 - \alpha_2^c,\ z_3 = e_3 - \alpha_3^c, \tag{32}$$

where $\alpha_i^c, i=2,3$ which are equivalent to $Z_{i,1}, i=2,3$ denote the outputs of FO command filter.

The compensated tracking errors are expressed as

$$\upsilon_i = z_i - \theta_i, i=1,2,3, \tag{33}$$

where θ_i denotes the compensating signal between virtual control and filtering signal.

The error variable is constrained by the following inequations

$$-\underline{\rho}\beta(t) < e_1 < \bar{\rho}\beta(t), \forall t \ge 0, \tag{34}$$

where $0 < \underline{\rho}, \bar{\rho} \le 1$.

Define a smooth and invertible function $S_1(z_1)$, the above inequation can be written in an unconstrained form as

$$e_1 = \beta(t) S_1(z_1). \tag{35}$$

It is noted that $\left(\bar{\rho}\mathbf{e}^{z} - \underline{\rho}\mathbf{e}^{-z}\right)/\left(\mathbf{e}^{z}+\mathbf{e}^{-z}\right)$ belongs to one of the said smooth and invertible functions.

Then the inverse transformation of (35) is written

$$z_1 = S_1^{-1}(\phi(t)), \tag{36}$$

where $\phi_1(t) = e_1(t)/\beta(t)$.

The FO derivative of (36) can be deduced as

$$\begin{aligned} {}^{C}\mathscr{D}_{0,t}^{\alpha} z_1 &= \left[{}^{C}\mathscr{D}_{z_1}^{\alpha} S_1(z_1)\beta(t)\right]^{-1}\left({}^{C}\mathscr{D}_{0,t}^{\alpha} e_1(t) - \phi_1(t)\,{}^{C}\mathscr{D}_{0,t}^{\alpha}\beta(t)\right) \\ &= \eta_1\left({}^{C}\mathscr{D}_{0,t}^{\alpha} e_1 - r_1\right), \end{aligned} \tag{37}$$

where $\eta_1 = \left[\beta(t)\cdot{}^{C}\mathscr{D}_{z_1}^{\alpha} S_1(z_1)\right]^{-1}$ and $r_1 = \phi_1(t)\,{}^{C}\mathscr{D}_{0,t}^{\alpha}\beta(t)$.

Remark 5: Due to $-1 < S_1(z_1) < 1$ and $\beta(t) > 0$, then $-\beta(t) < S_1(z_1)\beta(t) < \beta(t)$. With (36), we can know that the error variable e_1 is restrained in $(-\beta(t), \beta(t))$. Then e_1 will be constrained within the set Δ_c after a finite-time, where $\Delta_c = \{e_1 \in \Re : |e_1| < \beta_{T_0},\ t \ge T_0\}$. Furthermore, $0 < \beta_{T_0} \le \beta(t) \le \beta(0)$ and $0 < {}^{C}\mathscr{D}_{z_1}^{\alpha} S_1(z_1) = 2(\underline{\rho}+\bar{\rho})/\left(\mathbf{e}^{z}+\mathbf{e}^{-z}\right)^2 \cdot {}^{C}\mathscr{D}_{t}^{\alpha} z_1 \le 1$. It can be obtained that $\left[\beta(t)\cdot{}^{C}\mathscr{D}_{z_1}^{\alpha} S_1(z_1)\right]^{-1} \ge \beta^{-1}(0)$.

With (15) and (37), there exist

$${}^{C}\mathscr{D}_{0,t}^{\alpha} z_1 = \eta_1\left(f_1 + \sigma e_2 - r_1\right), {}^{C}\mathscr{D}_{0,t}^{\alpha} e_2 = f_2 + u_2, {}^{C}\mathscr{D}_{0,t}^{\alpha} e_3 = f_3 + u_3 \tag{38}$$

where $f_1 = -\rho e_1$, $f_2 = -e_2 - y_1 y_3 + x_1 x_3 - (\boldsymbol{\kappa}_1 e_1 + \boldsymbol{\kappa}_2 e_2) H(t - t_g) + \mu e_1$ and $f_3 = -e_3 + y_1 y_2 - x_1 x_2$ are generally regarded as unknown functions due to fluctuations originated from wind speed, generator temperature, stator resistance, friction coefficient and work load.

Based on the principle of FO backstepping, the proposed controller is composed of three steps.

Step 1: In view of the uncertainty of f_1, to facilitate controller design, the above-mentioned HT2FNN is used to estimate it over a compact set, namely

$$f_1 = w_1^{\mathrm{T}}\xi_1(\cdot) + \varepsilon_1(\cdot), \tag{39}$$

where $(\cdot)$ denotes the abbreviation of (x_1, x_2, x_3).

Select the first Lyapunov function candidate

$$V_1 = \frac{1}{2}\upsilon_1^2 + \frac{1}{2}\tilde{\zeta}_1^2 + \frac{1}{2}\theta_1^2. \tag{40}$$

Taking the FO derivative of V_1, it yields

$$\begin{aligned} &{}^{C}\mathscr{D}_{0,t}^{\alpha} V_1 \le \upsilon_1\eta_1\left[f_1 + \bar{\sigma}\left(z_2 + \alpha_2^v + \alpha_2^c - \alpha_2^v\right) - r_1\right] - \upsilon_1\,{}^{C}\mathscr{D}_{0,t}^{\alpha}\theta_1 - \tilde{\zeta}_1 \cdot \\ &{}^{C}\mathscr{D}_{0,t}^{\alpha}\hat{\zeta}_1 + \theta_1\,{}^{C}\mathscr{D}_{0,t}^{\alpha}\theta_1, \\ &\le \upsilon_1\eta_1\left[\upsilon_1\eta_1\hat{\zeta}_1\xi_1^{\mathrm{T}}(\cdot)\xi_1(\cdot)/2b_1^2 + \varepsilon_1 + \bar{\sigma}z_2 + \bar{\sigma}\alpha_2^v + \bar{\sigma}\left(\alpha_2^c - \alpha_2^v\right) - r_1\right] \\ &-\upsilon_1\,{}^{C}\mathscr{D}_{0,t}^{\alpha}\theta_1 + \theta_1\,{}^{C}\mathscr{D}_{0,t}^{\alpha}\theta_1 + b_1^2/2 + \tilde{\zeta}_1\left(\upsilon_1^2\eta_1^2\xi_1^{\mathrm{T}}(\cdot)\xi_1(\cdot)/2b_1^2 - {}^{C}\mathscr{D}_{0,t}^{\alpha}\hat{\zeta}_1\right) \end{aligned} \tag{41}$$

where α_2^v and $\bar{\sigma}$ are the virtual control and upper bound of σ, $\zeta_1 = \|w_1\|^2$ and $b_1 > 0$.

By invoking the Definition 2, the following cost function is designed to achieve its minimum as

$$\bar{J}_i = \int_0^{\infty}\left(\upsilon_i^2 + \delta_i^2\upsilon_i^2 + \kappa_i^2 u_{oi}^2\right)\mathrm{d}t,\ i=2,3, \tag{42}$$

where u_{oi}, δ_i^2 and κ_i represent the optimal control input, positive constant and design parameter. To compensate the approximating error of the HT2FNN, the inequations hold such that $\varepsilon_i^2(\cdot) \le \delta_i^2\upsilon_i^2$, $i=1,2,3$.

The optimal control inputs are designed as $u_{oi} = -\mathrm{P}_i\upsilon_i/\kappa_i^2, i=1, 2,3$ wherein P_i belongs to the solution of algebraic Riccati equation $\mathrm{P}_i^2 + 2k_i\mathrm{P}_i - \kappa_i^2 - 1 = 0$, $k_i > 0$.

Then the optimal control inputs are further deduced

$$u_{oi} = -\left(\sqrt{1 + k_i^2 + \delta_i^2} - k_i\right)\upsilon_i/\kappa_i^2, i=1,2,3. \tag{43}$$

The virtual control, its adaptive law and compensating signal are chosen accordingly

$$\alpha_2^v = \left(-k_1 z_1 - \upsilon_1\eta_1\hat{\zeta}_1\xi_1^{\mathrm{T}}(\cdot)\xi_1(\cdot)/2b_1^2 + r_1 - \mathrm{s}_1\upsilon_1^{\gamma} + u_{o1}\right)/\bar{\sigma}, \tag{44}$$

$${}^{C}\mathscr{D}_{0,t}^{\alpha}\hat{\zeta}_1 = \upsilon_1^2\eta_1^2\xi_1^{\mathrm{T}}(\cdot)\xi_1(\cdot)/2b_1^2 - \gamma_1\hat{\zeta}_1, \tag{45}$$

$${}^{C}\mathscr{D}_{0,t}^{\alpha}\theta_1 = -k_1\eta_1\theta_1 + \bar{\sigma}\eta_1\left(\alpha_2^c - \alpha_2^v + \theta_2\right) - l_1\theta_1^{\gamma}, \tag{46}$$

where $k_1 > 0$, $l_1 > 0$, $\gamma_1 > 0$, $\mathrm{s}_1 > 0$, $0 < \gamma < 1$.

With (5), substituting (44)-(46) into (41) yields

$$\begin{aligned} &{}^{C}\mathscr{D}_{0,t}^{\alpha} V_1 \le -k_1\eta_1\upsilon_1^2 - k_1\eta_1\theta_1^2 + \bar{\sigma}\eta_1\upsilon_1\upsilon_2 + \bar{\sigma}\eta_1\theta_1\theta_2 + \bar{\sigma}\eta_1\left(\theta_1^2 + \Gamma_{2,1}^2\right)/2 \\ &+ b_1^2/2 + \gamma_1\hat{\zeta}_1\tilde{\zeta}_1 + \eta_1\upsilon_1^2\left(1/2 + \delta_1^2/2 - \left(\sqrt{1 + k_1^2 + \delta_1^2} - k_1\right)/\kappa_1^2\right) \\ &-b_1\left|\upsilon_1\right|^{\gamma+1} - d_1\left|\theta_1\right|^{\gamma+1}, \end{aligned} \tag{47}$$

where $b_1 = \mathrm{s}_1\eta_1 - l_1\vartheta_1/(\gamma+1)$ and $d_1 = l_1\left(1 - \gamma\vartheta_1^{-1/\gamma}/(\gamma+1)\right)$.

Step 2: To tackle the uncertain f_2 mentioned before, we use an HT2FNN to approximate it in the following form

$$f_2 = w_2^{\mathrm{T}}\xi_2(\cdot) + \varepsilon_2(\cdot). \tag{48}$$

Consider the second Lyapunov function candidate as

$$V_2 = V_1 + \frac{1}{2}\upsilon_2^2 + \frac{1}{2}\tilde{\zeta}_2^2 + \frac{1}{2}\theta_2^2. \tag{49}$$

The FO derivative of V_2 is written

$$
\begin{aligned}
&{}^{C}\mathscr{D}_{0,t}^{\alpha}V_2 \le -k_1\eta_1\upsilon_1^2 - k_1\eta_1\theta_1^2 + \bar{\sigma}\eta_1\left(\theta_1^2+\Gamma_{2,1}^2\right)/2 + \sum_{i=1}^{2} b_i^2/2 + \gamma_1\hat{\zeta}_1\tilde{\zeta}_1 \\
&-d_1\left|\theta_1\right|^{\gamma+1} + \upsilon_2\left(\hat{\zeta}_2\upsilon_2\xi_2^{\mathrm{T}}(\cdot)\xi_2(\cdot)/2b_2^2 + u_2 + \varepsilon_2 + \bar{\sigma}\eta_1 z_1 - {}^{C}\mathscr{D}_{0,t}^{\alpha}\alpha^{c}\right) - \upsilon_2\cdot \\
&{}^{C}\mathscr{D}_{0,t}^{\alpha}\theta_2 + \theta_2\left(\bar{\sigma}\eta_1\theta_1 + {}^{C}\mathscr{D}_{0,t}^{\alpha}\theta_2\right) + \tilde{\zeta}_2\left(\upsilon_2^2\xi_2^{\mathrm{T}}(\cdot)\xi_2(\cdot)/2b_2^2 - {}^{C}\mathscr{D}_{0,t}^{\alpha}\hat{\zeta}_2\right) - \\
&b_1\left|\upsilon_1\right|^{\gamma+1} - \bar{\sigma}\eta_1\upsilon_2\theta_1 + \eta_1\upsilon_1^2\left(1/2+\delta_1^2/2-\left(\sqrt{1+k_1^2+\delta_1^2}-k_1\right)/\kappa_1^2\right),
\end{aligned}
\tag{50}
$$

where $\zeta_2 = \left\|w_2\right\|^2$ and $b_2 > 0$.

The q-axis control input, its adaptive law and compensating signal are designed as

$$
u_2 = -k_2 z_2 - \bar{\sigma}\eta_1 z_1 - \frac{\hat{\zeta}_2}{2b_2^2}\upsilon_2\xi_2^{\mathrm{T}}(\cdot)\xi_2(\cdot) + {}^{C}\mathscr{D}_{0,t}^{\alpha}\alpha_2^{c} - s_2\upsilon_2^{\gamma} + u_{o2}, \tag{51}
$$

$$
{}^{C}\mathscr{D}_{0,t}^{\alpha}\hat{\zeta}_2 = \upsilon_2^2\xi_2^{\mathrm{T}}(\cdot)\xi_2(\cdot)/2b_2^2 - \gamma_2\hat{\zeta}_2, \tag{52}
$$

$$
{}^{C}\mathscr{D}_{0,t}^{\alpha}\theta_2 = -k_2\theta_2 - \bar{\sigma}\eta_1\theta_1 - l_2\theta_2^{\gamma}, \tag{53}
$$

where $k_2 > 0$, $l_2 > 0$, $\gamma_2 > 0$ and $s_2 > 0$.

With (5), (51)-(53), (50) is further simplified as

$$
\begin{aligned}
&{}^{C}\mathscr{D}_{0,t}^{\alpha}V_2 \le -k_1\eta_1\upsilon_1^2 - k_2\upsilon_2^2 - k_1\eta_1\theta_1^2 - k_2\theta_2^2 + \bar{\sigma}\eta_1\left(\theta_1^2+\Gamma_{2,1}^2\right)/2 + \sum_{i=1}^{2}\frac{b_i^2}{2} \\
&+\sum_{i=1}^{2}\gamma_i\hat{\zeta}_i\tilde{\zeta}_i + \eta_1\upsilon_1^2\left(1/2+\delta_1^2/2-\left(\sqrt{1+k_1^2+\delta_1^2}-k_1\right)/\kappa_1^2\right) - \sum_{i=1}^{2} d_i\cdot \\
&\left|\theta_i\right|^{\gamma+1} - \sum_{i=1}^{2} b_i\left|\upsilon_i\right|^{\gamma+1} + \upsilon_2^2\left(\frac{1}{2}+\frac{\delta_2^2}{2}-\frac{1}{\kappa_2^2}\left(\sqrt{1+k_2^2+\delta_2^2}-k_2\right)\right),
\end{aligned}
\tag{54}
$$

where $b_1 = s_2 - l_2\vartheta_2/(\gamma+1)$ and $d_2 = l_2\left(1-\gamma\vartheta_2^{-1/\gamma}/(\gamma+1)\right)$.

Step 3: Similarly, to deal with an unknown function f_3, we borrow an HT2FNN to estimate it with a high degree of accuracy and repeatability as

$$
f_3 = w_3^{\mathrm{T}}\xi_3(\cdot) + \varepsilon_3(\cdot). \tag{55}
$$

α_3^{c} equals to zero since it adopts the flux-oriented control. Then define the last Lyapunov function candidate as

$$
V_3 = V_2 + \frac{1}{2}\upsilon_3^2 + \frac{1}{2}\tilde{\zeta}_3^2 + \frac{1}{2}\theta_3^2. \tag{56}
$$

Computing the FO derivative of V_3, it has

$$
\begin{aligned}
&{}^{C}\mathscr{D}_{0,t}^{\alpha}V_3 \le -k_1\eta_1\upsilon_1^2 - k_2\upsilon_2^2 - k_1\eta_1\theta_1^2 - k_2\theta_2^2 + \bar{\sigma}\eta_1\left(\theta_1^2+\Gamma_{2,1}^2\right)/2 + \\
&\sum_{i=1}^{3} b_i^2/2 + \sum_{i=1}^{2}\gamma_i\hat{\zeta}_i\tilde{\zeta}_i - \sum_{i=1}^{2} d_i\left|\theta_i\right|^{\gamma+1} - \sum_{i=1}^{2} b_i\left|\upsilon_i\right|^{\gamma+1} + \theta_3\,{}^{C}\mathscr{D}_{0,t}^{\alpha}\theta_3 + \upsilon_3\cdot \\
&\left(\hat{\zeta}_3\upsilon_3\xi_3^{\mathrm{T}}(\cdot)\xi_3(\cdot)/2b_3^2 + u_3 + \varepsilon_3\right) + \tilde{\zeta}_3\left(\upsilon_3^2\xi_3^{\mathrm{T}}(\cdot)\xi_3(\cdot)/2b_3^2 - {}^{C}\mathscr{D}_{0,t}^{\alpha}\hat{\zeta}_3\right) \\
&+\eta_1\upsilon_1^2\left(1/2+\delta_1^2/2-\left(\sqrt{1+k_1^2+\delta_1^2}-k_1\right)/\kappa_1^2\right) - \upsilon_3\,{}^{C}\mathscr{D}_{0,t}^{\alpha}\theta_3 + \upsilon_2^2\cdot \\
&\left(1/2+\delta_2^2/2-\left(\sqrt{1+k_2^2+\delta_2^2}-k_2\right)/\kappa_2^2\right),
\end{aligned}
\tag{57}
$$

where $\zeta_3 = \left\|w_3\right\|^2$ and $b_3 > 0$.

Then the d-axis control input, its adaptive law and compensating signal are designed as

$$
u_3 = -k_3 z_3 - \hat{\zeta}_3\upsilon_3\xi_3^{\mathrm{T}}(\cdot)\xi_3(\cdot)/2b_3^2 - s_3\upsilon_3^{\gamma} + u_{o3}, \tag{58}
$$

$$
{}^{C}\mathscr{D}_{0,t}^{\alpha}\hat{\zeta}_3 = \upsilon_3^2\xi_3^{\mathrm{T}}(\cdot)\xi_3(\cdot)/2b_3^2 - \gamma_3\hat{\zeta}_3, \tag{59}
$$

$$
{}^{C}\mathscr{D}_{0,t}^{\alpha}\theta_3 = -k_3\theta_3 - l_3\theta_3^{\gamma}, \tag{60}
$$

where $k_3 > 0$, $l_3 > 0$, $\gamma_3 > 0$ and $s_3 > 0$.

It can be drawn from (5), (58)-(60) that

$$
\begin{aligned}
&{}^{C}\mathscr{D}_{0,t}^{\alpha}V_3 \le -k_1\eta_1\upsilon_1^2 - \sum_{i=2}^{3}k_i\upsilon_i^2 - k_1\eta_1\theta_1^2 - \sum_{i=2}^{3}k_i\theta_i^2 + \bar{\sigma}\eta_1\left(\theta_1^2+\Gamma_{2,1}^2\right)/2 \\
&+\eta_1\upsilon_1^2\left(1/2+\delta_1^2/2-\left(\sqrt{1+k_1^2+\delta_1^2}-k_1\right)/\kappa_1^2\right) - \sum_{i=1}^{3} b_i\left|\upsilon_i\right|^{\gamma+1} \\
&+\sum_{i=2}^{3}\upsilon_i^2\left(\frac{1}{2}+\frac{\delta_i^2}{2}-\frac{1}{\kappa_i^2}\left(\sqrt{1+k_i^2+\delta_i^2}-k_i\right)\right) + \sum_{i=1}^{3} b_i^2/2 + \sum_{i=1}^{3}\gamma_i\hat{\zeta}_i\tilde{\zeta}_i \\
&-\sum_{i=1}^{3} d_i\left|\theta_i\right|^{\gamma+1},
\end{aligned}
\tag{61}
$$

where $b_3 = s_3 - l_3\vartheta_3/(\gamma+1)$ and $d_3 = l_3\left(1-\gamma\vartheta_3^{-1/\gamma}/(\gamma+1)\right)$.

Remark 6: The filtering errors of the FO finite-time command filter will become unmanageable when the order of complex nonlinear system increases. In this case, it is tricky to obtain a smallest possible tracking error. So, it is necessary and meaningful to construct the compensating signal to solve one such issue together with achieving finite-time convergence.

To clearly show the structure of our scheme, the block diagram is presented in Fig.9.

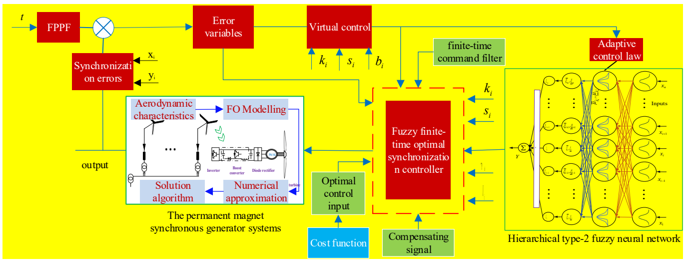

Fig.9.The block diagram of the proposed scheme.

V. Stability analysis

Theorem 1: Considering the unidirectionally coupled FO PMSGs with chaotic oscillation, if the q- and d-axis control inputs with adaptive laws (52), (59) and compensating signals (53), (60) are designed as (51) and (58), the all signals in closed-loop system are uniformly ultimately bounded and the synchronization errors involving the stability satisfy the presupposed performance condition. Meanwhile, the purpose of the fuzzy finite-time optimal synchronization control is achieved, and the cost function is minimized.

Proof. Define the entire Lyapunov function candidate

$$
V_e = \frac{1}{2}\sum_{i=1}^{3}\upsilon_i^2 + \frac{1}{2}\sum_{i=1}^{3}\tilde{\zeta}_i^2 + \frac{1}{2}\sum_{i=1}^{3}\theta_i^2. \tag{62}
$$

The corresponding FO derivative of (62) can be derived

$$
\begin{aligned}
&{}^{C}\mathscr{D}_{0,t}^{\alpha}V_e \le -k_1\eta_1\upsilon_1^2 - \sum_{i=2}^{3}k_i\upsilon_i^2 - \eta_1\left(k_1-\bar{\sigma}/2\right)\theta_1^2 - \sum_{i=2}^{3}k_i\theta_i^2 + \bar{\sigma}\eta_1\Gamma_{2,1}^2/2 \\
&+\eta_1\upsilon_1^2\left(1/2+\delta_1^2/2-\left(\sqrt{1+k_1^2+\delta_1^2}-k_1\right)/\kappa_1^2\right) + \sum_{i=1}^{3} b_i^2/2 - \sum_{i=1}^{3} d_i\left|\theta_i\right|^{\gamma+1} \\
&+\sum_{i=2}^{3}\upsilon_i^2\left(1/2+\delta_i^2/2-\left(\sqrt{1+k_i^2+\delta_i^2}-k_i\right)/\kappa_i^2\right) - \sum_{i=1}^{3} b_i\left|\upsilon_i\right|^{\gamma+1} + \\
&\sum_{i=1}^{3}\gamma_i\zeta_i^2/2 - \sum_{i=1}^{3}\gamma_i\tilde{\zeta}_i^2/2 \le -a_e V_e - b_e V_e^{(\gamma+1)/2} + c_e,
\end{aligned}
\tag{63}
$$

where $a_e = 2\min\left\{\begin{matrix}\eta_1\left(k_1-\bar{\sigma}/2\right), \eta_1\left(k_1-\psi_1\right), k_2+\psi_2, k_3+\psi_3, \\ \gamma_1/2, \gamma_2/2, \gamma_3/2\end{matrix}\right\}$,

$b_e = 2\min\{d_1,b_1,d_2,b_2,d_3,b_3\}$ and $c_e = \bar{\sigma}\eta_1\Gamma_{2,1}^2/2+\sum_{i=1}^{3}\gamma_i\zeta_i^2/2$ with $\psi_1 = \eta_1\left(1/2+\delta_1^2/2-\left(\sqrt{1+k_1^2+\delta_1^2}-k_1\right)/\kappa_1^2\right)$, $\psi_2 = \upsilon_2^2\left(1/2+\delta_2^2/2-\left(\sqrt{1+k_2^2+\delta_2^2}-k_2\right)/\kappa_2^2\right)$ and $\psi_3 = \upsilon_3^2\left(1/2+\delta_3^2/2-\left(\sqrt{1+k_3^2+\delta_3^2}-k_3\right)/\kappa_3^2\right)$.

υ_i, $\tilde{\zeta}_i$ and θ_i achieve the stability in T_0 within a compact set Ω_e as

$$\Omega_e := \left\{\upsilon_i \in \mathbb{R},\theta_i \in \mathbb{R},\tilde{\zeta}_i \in \mathbb{R}, i=1,2,3 \middle| \upsilon_i^2+\tilde{\zeta}_i^2+\theta_i^2 \le D_e\right\}, \quad (64)$$

where $D_e = \min\left\{c_e/(1-\lambda_e)a_e, \left(c_e/(1-\lambda_e)b_e\right)^{2/(\gamma+1)}\right\}$ with $0<\lambda_e<1$.

The finite-time T_0 can be given as

$$T_0 \le \max\{t_1,t_2\}, \quad (65)$$

where $t_1 = \ln\left(\left(\lambda_e a_e V_e^{1-(1+\lambda_e)/2}(0)+b_e\right)/b_e\right)/\lambda_e a_e\left(1-(1+\lambda_e)/2\right)$, $t_2 = \ln\left(\left(a_e V_e^{1-(1+\lambda_e)/2}(0)+\lambda_e b_e\right)/\lambda_e b_e\right)/a_e\left(1-(1+\lambda_e)/2\right)$.

This completes the proof.

VI. Simulation results and discussion

The coupling parameters between the master and slave PMSGs are given as $\boldsymbol{\kappa}_1 = 0.1$, $\boldsymbol{\kappa}_2 = -0.1$. The parameters of the finite-time preconfigured performance function are chosen as $a_0 = 0.4$, $a_1 = 0$, $a_2 = -4.9$, $a_3 = 6.3$ and $\beta_{T_0} = 0.02$. The finite-time is set to $T_0 = 0.4$. The parameters of the FO finite-time command filter are set to $\boldsymbol{c}_{1,1} = 6$ and $\boldsymbol{c}_{1,2} = 5$. The parameters of the smooth and invertible function are defined as $\underline{\rho} = 0.1$ and $\bar{\rho} = 1$. The controller parameters are selected as $k_1 = k_2 = k_3 = 10$, $\gamma_1 = \gamma_2 = 2$, $\gamma_3 = 8$, $l_1 = l_2 = l_3 = 10$, $s_1 = s_2 = s_3 = 0.5$, $\delta_1^2 = \delta_2^2 = \delta_3^2 = 2$, $\gamma = 0.4$, $b_1 = b_2 = b_3 = 1$ and $\kappa_1 = \kappa_2 = \kappa_3 = 1$. Finally, the centers of the MGs associated with the HT2FNN are evenly distributed in the interval [-1,1], and the upper/lower width of MGs is chosen as $\bar{\sigma}_{\tilde{A}_i^j} = 0.06$, $\underline{\sigma}_{\tilde{A}_i^j} = 0.02$.

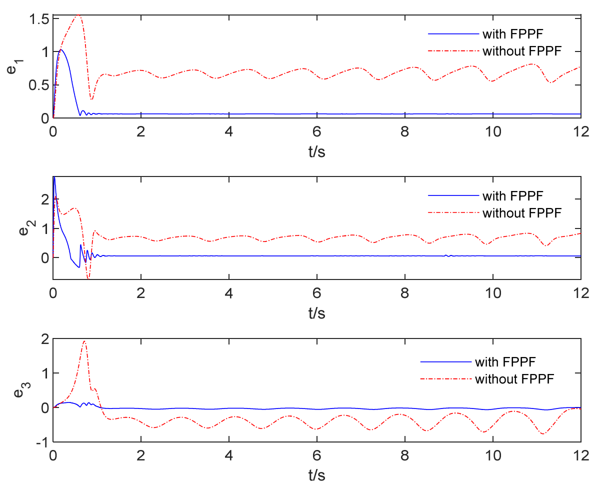

Fig.10. Synchronization errors with- and without- FPPF under same conditions.

Fig.10 shows the synchronization errors of unidirectionally coupled FO PMSGs with FPPF (blue curve) and without FPPF (red curve). It is very obvious that the traditional scheme without FPPF has a large overshoot and a long oscillation period in the whole operation process. But our scheme implements fast synchronization between master and slave PMSGs with a small error in a finite time. Therefore, our scheme obviously exceeds the scheme without FPPF under the same conditions.

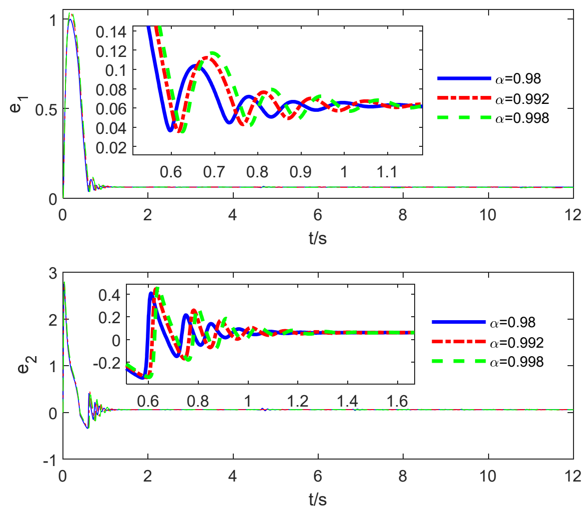

Fig.11. The synchronization errors for different FOs.

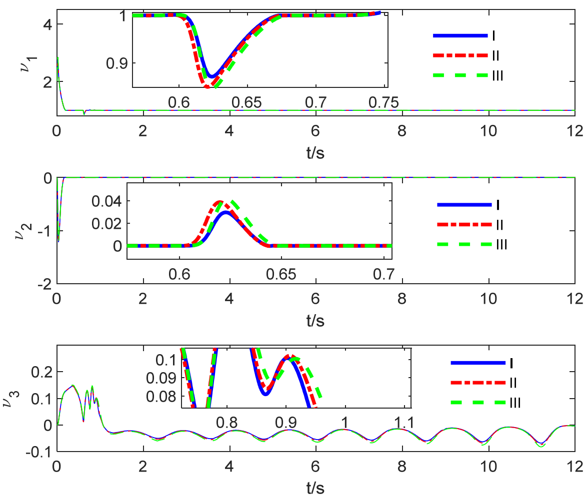

Fig.12. The compensating tracking errors for different coupling parameters.

The real-time changes of the power grid caused by the surrounding environment do have inevitable effect on working conditions of every generator through the transmission bus and each feeder of the wind farm. This fact can give rise to inaccurate modeling and system parameter perturbation. Fig.11 reveals that the proposed scheme overcomes these adverse effects better. The alternating current master and slave PMSGs achieve exact coincidence of frequencies for common loading. The motion states of slave PMSG are sucked to the attraction basin of master PMSG in the shortest possible time. Meanwhile the synchronization errors are controlled within the boundaries of pre-configured performance.

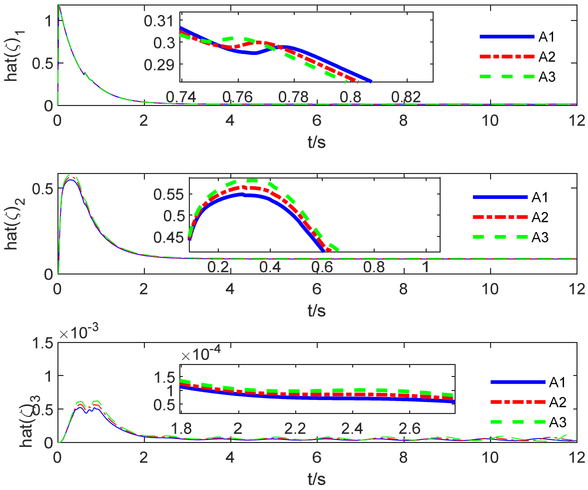

Fig.13. The switched weights for different system parameters.

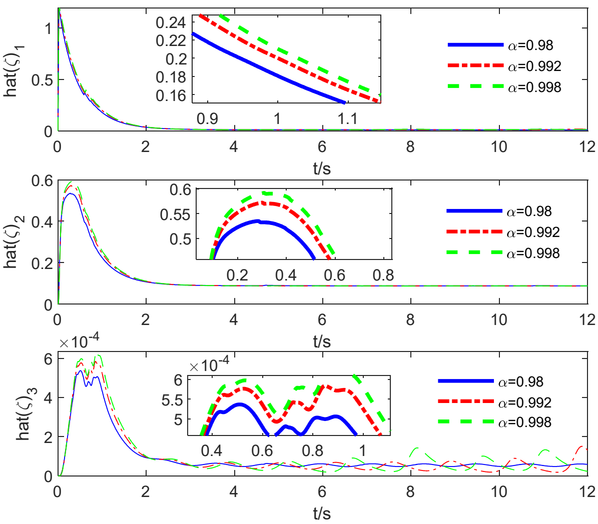

Fig.14. The switched weights for different FOs.

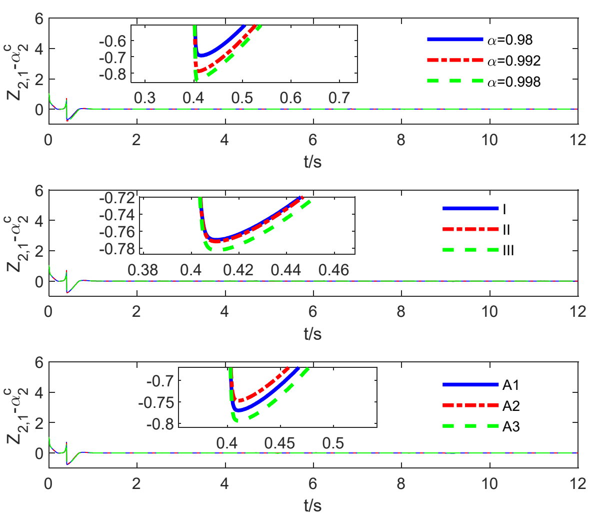

Fig.15. The performance of the FO finite-time command filter under different cases.

The space of coupling coefficients can directly determine the synchronization/desynchrony and harmonic oscillation/cyclic motion of generators operating in parallel mode. Three combinations are hence given such as I: $\boldsymbol{\kappa}_1=0.1$, $\boldsymbol{\kappa}_2=-0.1$; II: $\boldsymbol{\kappa}_1=0.2$, $\boldsymbol{\kappa}_2=-0.15$; III: $\boldsymbol{\kappa}_1=0.15$, $\boldsymbol{\kappa}_2=-0.2$. In three cases, the PMSG can generate oscillatory behaviors before the proposed method intervenes. Fig.12 depicts the compensating tracking errors for different coupling parameters after our scheme gets involved. It can be seen that several curves are overlapped over all time. The presented method processes strong capacity of resisting disturbance associated with coupling coefficient.

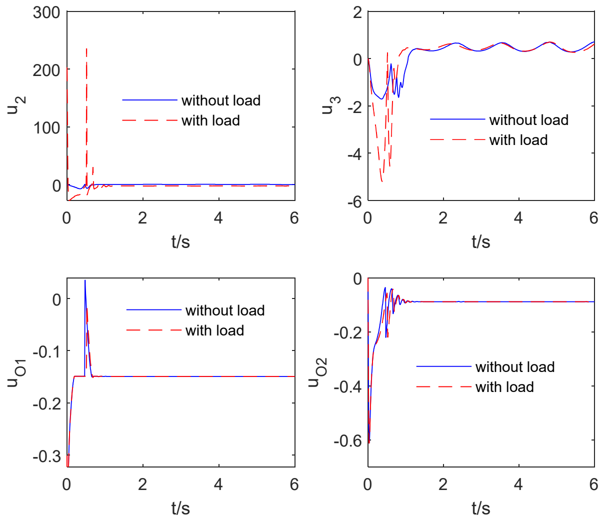

Fig.16. The q-/d- axis control input and optimal control input with and without the generator torque $T_L=10$ at the beginning.

The HT2FNN with a transformation plays an important role in function approximation to tackle fluctuation problem originated from wind speed, generator temperature, stator resistance, friction coefficient and work load. Three sets of system parameter perturbation are hence defined such as A1: $\rho=5$, $\mu=19$; A2: $\rho=5.5$, $\mu=20$; A3: $\rho=6$, $\mu=21$. From Figs.13-14, the switched weights of the HT2FNN converge quickly to a small neighborhood of the origin in self-structuring algorithm. Meanwhile, three curves always overlap, whether it is in different system parameters or different FOs.

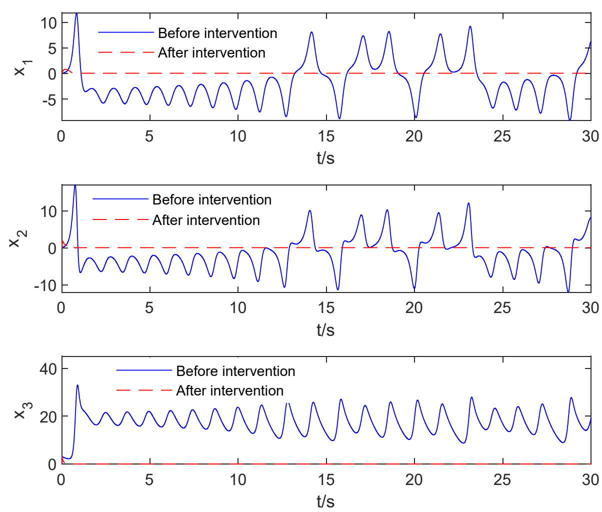

Fig.17. Chaos suppression capability.

The FO finite-time command filter matched up with the compensating signal can achieve the purposes of faster response, precise estimate and finite-time convergence. Fig.15 fully shows its high performance regardless of whether there exist variational coupling coefficients, system parameters perturbations or changed FOs.

Fig.16 exhibits the control input and optimal control input with and without the external load at the moment of startup. It is obvious that the unidirectionally coupled FO PMSG system under load quickly achieve stable operation after a brief fluctuation. Therefore, the constructed controller processes good anti-disturbance capacity.

Form Fig.17, the PMSG can generate abundant dynamical behaviors including chaotic oscillations when the effective control methods do not yet plug into the system. Each PMSG immediately switches to regular motion in 0.4 second once the proposed fuzzy finite-time optimal control scheme gets involved. The corresponding chaotic oscillations are completely suppressed here.

VII. Conclusion

This paper studies dynamic analysis and the fuzzy finite-time optimal synchronization control issue of unidirectionally coupled FO PMSG system. Based on the constructed synchronization model, the dynamic analysis fully shows abundant dynamical behaviors of system by phase portrait and Lyapunov exponent and gives stability/instability boundaries with numerical method. Then a fuzzy finite-time optimal synchronization control scheme fusing with the HT2FNN, finite-time command filter, finite-time preconfigured performance function and optimal control is proposed in the framework of backstepping. The designed scheme can not only guarantee the boundness of all signals of the concerned closed-loop system and stable operation with performance constraint, but also reach purposes of finite-time synchronization and minimizing cost function. Meanwhile, it can enable the slave PMSG to oblige from its own orbit to accurately follow that of master PMSG in the shortest possible time. In the subsequent study, we will focus more on the event-triggered optimal synchronization control of the FO PMSG in networks.

Acknowledgment

This project is supported by National Natural Science Foundation of China (Nos. 52065008, 61860206008 and 61933012), Science and Technology Planning Project of Guizhou Province (No. [2021]5634), Science and Technology Research Program of Chongqing Municipal Education Commission (No. KJZD-M202 100101) and Innovation and Entrepreneurship Program for High-Level Talents of Guizhou Province (No. (2021)08).

Conflict of interest

The authors declare that they have no known competing financial interests or personal relationships that could have appeared to influence the work reported in this paper.

References

[1]L. Shanmugam and Y. H. Joo, "Stabilization of permanent magnet synchronous generator-based wind turbine system via fuzzy-based sampled-data control approach," *Inform. Sciences,* vol. 559, pp. 270-285, 2021.

[2]J. Yang, H. Yan, C. Gu, S. Wang, and G. Buticchi, "Modeling and stability enhancement of a permanent magnet synchronous generator based DC system for more electric aircraft," *IEEE Trans.Ind. Electron.,* p. DOI: 10.1109/TIE.2021.3066934, 2021.

[3]M. Prakash and Y. H. Joo, "Fuzzy event-triggered control for back to back converter involved PMSG-based wind turbine systems," *IEEE Trans. Fuzzy Syst.,* p. DOI: 10.1109/TFUZZ.2021.3059949, 2021.

[4]S. Luo, X. Hu, L. Zhao, and S. Li, "Event-triggered neural adaptive backstepping control of the K chaotic PMSGs coupled system," *Int. J. Elec. Power Energ. Syst.,* vol. 135, p. 107475, 2022.

[5]G. Si, J. Zhu, L. Diao, and Z. Ding, "Modeling, nonlinear dynamic analysis and control of fractional PMSG of wind turbine," *Nonlinear Dyn.,* vol. 88, no. 2, pp. 985-1000, 2017.

[6]A. Ardjal, A. Merabet, M. Bettayeb, R. Mansouri, and L. Labib, "Design and implementation of a fractional nonlinear synergetic controller for generator and grid converters of wind energy conversion system," *Energy,* vol. 186, no. 1, p. 115861, 2019.

[7]S. Luo, Y. Song, F. L. Lewis, and R. Garrappa, "Neuroadaptive optimal fixed-time synchronization and its circuit realization for unidirectionally coupled FO self-sustained electromechanical seismograph systems," *IEEE Trans. Cybern.,* no. DOI: 10.1109/TCYB.2021.3121069, 2021.

[8]B. Xu, D. Chen, H. Zhang, and R. Zhou, "Dynamic analysis and modeling of a novel fractional-order hydro-turbine-generator unit," *Nonlinear Dyn.,* vol. 81, no. 3, pp. 1263-1274, 2015.

[9]S. He, K. Sun, and X. Wu, "Fractional symbolic network entropy analysis for the fractional-order chaotic systems," *Phys. Scr.,* vol. 95, no. 3, p. 035220, 2020.

[10]S. Westerlund and L. Ekstam, "Capacitor theory," *IEEE Trans. Dielect. Electr. In.,* vol. 1, no. 5, pp. 826-839, 1994.

[11]Y. Luo, Y. Q. Chen, and Y. Pi, "Experimental study of fractional order proportional derivative controller synthesis for fractional order systems," *Mechatronics,* vol. 21, no. 1, pp. 204-214, 2011.

[12]M. Borah and B. K. Roy, "Dynamics of the Fractional-order Chaotic PMSG, its Stabilisation using Predictive Control and Circuit Validation," *IET Elec. Pow. Appl.,* vol. 11, no. 5, pp. 707-716, 2017.

[13]D. Tong, W. Zhou, X. Zhou, J. Yang, L. Zhang, and Y. Xu, "Exponential synchronization for stochastic neural networks with multi-delayed and Markovian switching via adaptive feedback control," *Commun. Nonlinear Sci. Numer. Simul.,* vol. 29, no. 1-3, pp. 359-371, 2015.

[14]S. Luo, F. L. Lewis, Y. Song, and H. M. Ouakad, "Optimal synchronization of unidirectionally coupled FO chaotic electromechanical devices with the hi-erarchical neural network " *IEEE Trans. Neural Netw. Learn. Syst.,* vol. 33, no. 3, pp. 1192-1202, 2022.

[15]D. Zhu, R. Wang, C. Liu, and J. Duan, "Synchronization of chaotic-oscillation permanent magnet synchronous generators networks via adaptive impulsive control," *IEEE Trans. Circuit. Syst.-II,* vol. 67, no. 10, pp. 2194-2198, 2020.

[16]S. He, K. Sun, and H. Wang, "Dynamics and synchronization of conformable fractional-order hyperchaotic systems using the Homotopy analysis method," *Commun. Nonlinear Sci. Numer. Simul.,* vol. 73, pp. 146-164, 2019.

[17]Jinling *et al.*, "Robust synchronization for 2-D discrete-time coupled dynamical networks," *IEEE Trans. Neural Netw. Learn. Syst.,* vol. 23, no. 6, pp. 942-953, 2012.

[18]Y. Yang and C. Z. Xu, "Adaptive fuzzy leader-follower synchronization of constrained heterogeneous multiagent systems," *IEEE Trans. Fuzzy Syst.,* vol. 28, no. 10, pp. 2389-2400, 2020.

[19]W. Wang, Y. Li, and S. Tong, "Adaptive fuzzy event-triggered control for leader-following consensus of high-order nonlinear systems," *IEEE Trans. Fuzzy Syst.,* vol. 28, no. 10, pp. 2389-2400, 2019.

[20]H. Fu, X. Chen, W. Wang, and M. Wu, "Data-based optimal synchronization control for discrete-time nonlinear heterogeneous multiagent systems," *IEEE Trans. Cybern.,* vol. PP, p. Doi: 10.1109/TCYB.2020.3004494., 2020.

[21]M. Li, J. Qin, Q. Ma, W. X. Zheng, and Y. Kang, "Hierarchical optimal synchronization for linear systems via reinforcement learning: a stackelberg-nash game perspective," *IEEE Trans. Neural Netw. Learn. Syst.,* vol. 32, no. 4, pp. 1600-1611, 2021.

[22]R. Sadeghi, S. M. Madani, and M. Ataei, "A new smooth synchronization of brushless doubly-fed induction generator by applying a proposed machine model," *IEEE Trans. Sustain. Energy,* vol. 9, no. 1, pp. 371-380, 2017.

[23]Y. Li, Y. Fan, K. Li, W. Liu, and S. Tong, "Adaptive optimized backstepping control-based RL algorithm for stochastic nonlinear systems with state constraints and its application," *IEEE Trans. Cybern.,* p. DOI: 10.1109/TCYB.2021.3069587, 2021.

[24]Y. D. Song, X. Huang, and Z. J. Jia, "Dealing with the issues crucially related to the functionality and reliability of NN-associated control for nonlinear uncertain systems," *IEEE Trans. Neural Netw. Learn. Syst.,* vol. 28, no. 11, pp. 2614-2625, 2017.

[25]S. Hou, J. Fei, C. Chen, and Y. Chu, "Finite-time adaptive fuzzy-neural-network control of active power filter," *IEEE Trans. Power Elect.,* vol. 34, no. 10, pp. 10298-10313, 2019.

[26]H. Liu, Y. Pan, J. Cao, Y. Zhou, and H. Wang, "Positivity and stability analysis for fractional-order delayed systems: A T-S fuzzy model approach," *IEEE Trans. Fuzzy Syst.,* p. DOI: 10.1109/TFUZZ.2020.2966420, 2020.

[27]Y. Wei, D. Sheng, Y. Chen, and Y. Wang, "Fractional order chattering-free robust adaptive backstepping control technique," *Nonlinear Dyn.,* vol. 95, no. 3, pp. 2383-2394, 2019.
[28]H. Modares, F. L. Lewis, and Z. P. Jiang, "H ∞ tracking control of completely unknown continuous-time systems via off-policy reinforcement learning," *IEEE Trans. Neural Netw. Learn. Syst.,* vol. 26, no. 10, pp. 2550-2562, 2015.
[29]K. G. Vamvoudakis and F. L. Lewis, "Multi-player non-zero-sum games: Online adaptive learning solution of coupled Hamilton–Jacobi equations," *Automatica,* vol. 47, no. 8, pp. 1556-1569, 2011.
[30]J. Sun and C. Liu, "Distributed fuzzy adaptive backstepping optimal control for nonlinear multi-missile guidance systems with input saturation," *IEEE Trans. Fuzzy Syst.,* vol. 27, no. 3, pp. 447-461, 2019.
[31]S. Luo, F. L. Lewis, Y. Song, and R. Garrappa, "Dynamical analysis and accelerated optimal stabilization of the fractional-order self-sustained electromechanical seismograph system with fuzzy wavelet neural network," *Nonlinear Dyn.,* vol. 104, no. 2, pp. 1389-1404, 2021.
[32]L. Wang, H. Wang, and P. X. Liu, "Adaptive fuzzy finite-time control of stochastic nonlinear systems with actuator faults," *Nonlinear Dyn.,* vol. 104, no. 1, 2021.
[33]S. Kuang, X. Guan, and D. Dong, "Finite-time stabilization control of quantum systems," *Automatica,* vol. 123, no. 11, p. 109327, 2021.
[34]P. Mani, J. H. Lee, K. W. Kang, and Y. H. Joo, "Digital controller design via LMIs for direct-driven surface mounted PMSG-based wind energy conversion system," *IEEE Trans. Cybern.,* vol. 50, no. 7, pp. 3056-3067, 2020.
[35]C. P. Bechlioulis and G. A. Rovithakis, "Adaptive control with guaranteed transient and steady state tracking error bounds for strict feedback systems," *Automatica,* vol. 45, no. 2, pp. 532-538, 2009.
[36]C. Liu, H. Wang, X. Liu, Y. Zhou, and S. Lu, "Adaptive prescribed performance tracking control for strict-feedback nonlinear systems with zero dynamics," *Int. J. Robust Nonlinear Contr.,* vol. 29, no. 18, pp. 6507-6521, 2019.
[37]Stamova and Ivanka, "Global Mittag-Leffler stability and synchronization of impulsive fractional-order neural networks with time-varying delays," *Nonlinear Dyn.,* vol. 77, no. 4, pp. 1251-1260, 2014.
[38]R. Garrappa, "Neglecting nonlocality leads to unreliable numerical methods for fractional differential equations," *Commun. Nonlinear Sci. Numer. Simul.,* vol. 70, pp. 302-306, 2019.
[39]K. Diethelm, R. Garrappa, and M. Stynes, "Good (and not so good) practices in computational methods for fractional calculus," *Mathematics,* vol. 8, no. 3, p. DOI:10.3390/math8030324, 2020.
[40]C. Qian and L. Wei, "Non-Lipschitz continuous stabilizers for nonlinear systems with uncontrollable unstable linearization," *Syst. Control Lett.,* vol. 42, no. 3, pp. 185-200, 2001.
[41]S. Luo, J. Li, S. Li, and J. Hu, "Dynamical analysis of the fractional-order centrifugal flywheel governor system and its accelerated adaptive stabilization with the optimality," *Int. J. Elec. Power Energ. Syst.,* vol. 118, p. 105792, 2020.
[42]R. Garrappa, "Numerical solution of fractional differential equations: A survey and a software tutorial," *Mathematics,* vol. 6, no. 2, p. 16, 2018.
[43]A. Mohammadzadeh and S. Ghaemi, "A modified sliding mode approach for synchronization of fractional-order chaotic/hyperchaotic systems by using new self-structuring hierarchical type-2 fuzzy neural network," *Neurocomputing,* vol. 191, pp. 200-213, 2016.
[44]A. Mohammadzadeh and S. Ghaemi, "Synchronization of chaotic systems and identification of nonlinear systems by using recurrent hierarchical type-2 fuzzy neural networks," *ISA Trans.,* vol. 58, pp. 318-329, 2015.
[45]J. Xia, B. Li, S. F. Su, W. Sun, and H. Shen, "Finite-time command filtered event-triggered adaptive fuzzy tracking control for stochastic nonlinear systems," *IEEE Trans. Fuzzy Syst.,* vol. 29, no. 7, pp. 1815-1825, 2021.

Shaohua Luo received the B.S., M.S. and Ph.D. degrees in Mechanical Engineering from Chongqing University, Chongqing, China, in 2005, 2009 and 2014, respectively.

He engaged in the postdoctoral research at Chongqing University from 2014 to 2016 in the field of adaptive control of dynamic systems.

He is currently a Professor at the State Key Laboratory of Public Big Date, Guizhou University. His research interests include the fractional-order electromechanical systems, mechanical & electrical transmission control, dynamic analysis, circuit realization, adaptive control and synchronization control of electromechanical systems. He is a provincial outstanding young scientific and technological talents, leader of provincial university innovation research group and special invited expert of "Enterprise Innovation Post". He has authored 14 China invention patents and 3 British invention patents and published more than 40 papers in the authoritative academic journals.

Yongduan Song (M'92–SM'10-F'20) received his Ph.D. degree in Electrical and Computer Engineering from Tennessee Technological University, Cookeville, USA, in 1992. He held a tenured Full Professor position with North Carolina A&T State University, Greensboro, from 1993 to 2008 and a Langley Distinguished Professor position with the National Institute of Aerospace, Hampton, VA, from 2005 to 2008.

He is now the Dean of School of Automation, Chongqing University, and the Founding Director of the Institute of Smart Systems and Renewable Energy, Chongqing University. He was one of the six Langley Distinguished Professors with the National Institute of Aerospace (NIA), Founding Director of Cooperative Systems at NIA. He has served as an Associate Editor/Guest Editor for several prestigious scientific journals. He has received several competitive research awards from the National Science Foundation, the National Aeronautics and Space Administration, the US Air Force Office, the US Army Research Office, and the US Naval Research Office. His research interests include intelligent systems, guidance navigation and control, bio-inspired adaptive and cooperative systems, rail traffic control and safety, and smart grid.

Frank L. Lewis (S'70-M'81-SM'86- F'94) received the bachelors degree in physics/electrical engineering and the M.S.E.E. degree in electrical engineering from Rice University, Houston in 1971, TX, USA, the M.S. degree in aeronautical engineering from the University of West Florida, Pensacola in 1977, FL, USA, and the Ph.D. degree in electrical engineering from the Georgia Institute of Technology in 1981, Atlanta, GA, USA.

He is currently a Distinguished Scholar Professor and Distinguished Teaching Professor with the University of Texas at Arlington, TX, USA, the Moncrief- ODonnell Chair of the University of Texas at Arlington Research Institute. He is involved in feedback control, intelligent systems, cooperative control systems, and nonlinear systems. He has authored six U.S. patents, numerous journal special issues, journal papers, and 20 books, including Optimal Control, Aircraft Control, Optimal Estimation, and Robot Manipulator Control.

Prof. Lewis is a member of the National Academy of Inventors, a fellow of the International Federation of Automatic Control and the Institute of Measurement and Control, U.K., a Texas Board of Professional Engineer, a U.K. Chartered Engineer, and a founding member of the Board of Governors of the Mediterranean Control Association. He was a recipient of the Fulbright Research Award, the NSF Research Initiation Grant, the Terman Award from the American Society for Engineering Education, the Gabor Award from the International Neural Network Society, the Honeywell Field Engineering Medal from the Institute of Measurement and Control, U.K., the Neural Networks Pioneer Award from IEEE Computational Intelligence Society, the Outstanding Service Award from the Dallas IEEE Section, and the Texas Regents

Outstanding Teaching Award in 2013. He was elected as an Engineer of the year by the Fort Worth IEEE Section. He was listed in the Fort Worth Business Press Top 200 Leaders in Manufacturing.

Roberto Garrappa was born in Monopoli (Italy) and received the B.Sc. degree in Computer Science from the University of Bari, Italy, in 1992.

After different working experiences in schools and universities, he was Researcher at the University of Bari from 2001 to 2015 and he is now Associate Professor in Numerical Analysis at the same University. His current research interests include numerical solution of ordinary and partial differential equations of integer and fractional (i.e., non-integer) order, evaluation of special functions, development of numerical software. He is author of several Matlab codes for fractional-order differential problems which are available in the MathWorks website.

Prof. Garrappa is member of the editorial board of Fractional Calculus and Applied Analysis, Applied Numerical Mathematics, Numerical Algorithms, Mathematics and Computers in Simulations, Computational and Applied Mathematics, Mediterranean Journal of Mathematics, and others. He is member of SIAM, SIMAI and UMI.

Shaobo Li received the B.S. and M.S. degrees of Mechanical Engineering in 1996 and 1999 from Huazhong University of Technology and Guizhou University of Technology University, China, respectively. He received the Ph.D. of Computer Engineering in 2003 from Chinese Academy of Sciences. He is currently a professor at the School of Mechanical Engineering, Guizhou University (GZU), China. He is also a part-time doctoral tutor at the Chinese Academy of Sciences, China.

From 2007 to 2015, he was the vice director of the Key Laboratory of Advanced Manufacturing Technology of Ministry of Education at GZU. He has been the dean of School of Mechanical Engineering at GZU since 2015. He published more than 200 papers in major journals and international conferences. His current research interests include big data of manufacturing, intelligent manufacturing. His research has been supported by National Science Foundation of China, National High-tech R&D Program (“863” Program), etc. He received honors and awards from New Century Excellent Talents in University of Ministry of Education of China, excellent expert and innovative talent of Guizhou Province, group leader of manufacturing informatization and alliance vice chairman of intelligent manufacturing industry in Guizhou Province, etc.